

Seasonal Variations of Carbonate Chemistry at Two Western Atlantic Coral Reefs

Melissa Meléndez¹ , Joseph Salisbury¹, Dwight Gledhill², Chris Langdon³ , Julio M. Morell^{4,5}, Derek Manzello⁶, Sylvia Rodriguez-Abudo^{4,5} , Sylvia Musielewicz^{7,8}, and Adrienne Sutton⁷ 

¹Department of Earth Sciences and Ocean Processes Analysis Laboratory, University of New Hampshire, Durham, NH, USA, ²National Oceanic and Atmospheric Administration (NOAA), Ocean Acidification Program, Silver Spring, MD, USA, ³Rosenstiel School of Marine and Atmospheric Science, University of Miami, Miami, FL, USA, ⁴Department of Marine Sciences, University of Puerto Rico, Mayagüez, PR, USA, ⁵Caribbean Coastal Ocean Observing System, NOAA, Magueyes Island, Lajas, PR, USA, ⁶Atlantic Oceanographic and Meteorological Laboratory, NOAA, Miami, FL, USA, ⁷Pacific Marine Environmental Laboratory, NOAA, Seattle, WA, USA, ⁸Joint Institute for the Study of the Atmosphere and Ocean, University of Washington, Seattle, WA, USA

Key Points:

- High-frequency carbonate data for two multi-year time series Florida and Puerto Rico show different seasonal amplitudes
- The seasonal cycle of carbonate chemistry reflects the combined effects of ecosystem processes and temperature dynamics
- Respiration, particularly in late summer and fall, is a major source of CO₂ to both systems

Supporting Information:

- Supporting Information S1

Correspondence to:

M. Meléndez,
mm19@wildcats.unh.edu

Citation:

Meléndez, M., Salisbury, J., Gledhill, D., Langdon, C., Morell, J. M., Manzello, D., et al. (2020). Seasonal variations of carbonate chemistry at two western Atlantic coral reefs. *Journal of Geophysical Research: Oceans*, 125, e2020JC016108. <https://doi.org/10.1029/2020JC016108>

Received 24 MAR 2020

Accepted 25 JUN 2020

Accepted article online 3 JUL 2020

Abstract Time series from open ocean fixed stations have robustly documented secular changes in carbonate chemistry and long-term ocean acidification (OA) trends as a direct response to increases in atmospheric carbon dioxide (CO₂). However, few high-frequency coastal carbon time series are available in reef systems, where most affected tropical marine organisms reside. Seasonal variations in carbonate chemistry at Cheeca Rocks (CR), Florida, and La Parguera (LP), Puerto Rico, are presented based on 8 and 10 years of continuous, high-quality measurements, respectively. We synthesized and modeled carbonate chemistry to understand how physical and biological processes affect seasonal carbonate chemistry at both locations. The results showed that differences in biology and thermodynamic cycles between the two systems caused higher amplitudes at CR despite the shorter residence times relative to LP. Analyses based on oxygen and temperature-normalized $p\text{CO}_{2\text{sw}}$ showed that temperature effects on $p\text{CO}_{2\text{sw}}$ at CR were largely counteracted by primary productivity, while thermodynamics alone explained a majority of the $p\text{CO}_{2\text{sw}}$ dynamics at LP. Heterotrophy dominated from late spring to fall, and autotrophy dominated from winter to early spring. Observations suggested that organic respiration decreased the carbonate mineral saturation state (Ω) during late summer/fall. The interactive effects between the inorganic and organic carbon cycles and the assumed effects of benthic metabolism on the water chemistry at both sites appeared to cause seasonal hysteresis with the carbonate chemistry. Improved integration of observational data to modeling approaches will help better forecast how physical and biogeochemical processes will affect Ω and carbonate chemistry in coastal areas.

Plain Language Summary Anthropogenic activities, such as the burning of fossil fuels, interact with the chemistry of the ocean surface and cause ocean acidification (OA). The current trend and projections for OA are well defined for open ocean waters, although less is known about its effects on nearshore ecosystems, where most of the affected organisms reside. In this work, we analyzed almost a decade of carbonate chemistry data for two reef time series at Cheeca Rocks (CR), Florida, and La Parguera (LP), Puerto Rico, to assess the physical and biological processes that dictate carbonate seasonal variability. The results showed that temperature is the dominant driver of seawater CO₂ changes at LP, while at CR, biological processes have major effects on CO₂ chemistry. Continued observations will advance future projections of OA in nearshore areas and provide coastal managers with appropriate tools to monitor OA.

1. Introduction

Changes in ocean chemistry as a direct response to rising atmospheric carbon dioxide (CO_{2atm}) concentrations are causing acidification of the surface and near-surface ocean (Caldeira & Wickett, 2003; Feely et al., 2004). As CO_{2atm} is absorbed by the ocean, it reacts with water (CO_{2aq}) to form carbonic acid, which rapidly dissociates to produce hydrogen ions [H⁺] (thereby lowering pH and hence the term “acidification”). This chemical process affects the degree to which seawater is saturated with respect to calcium carbonate (CaCO₃) mineral phases, as indicated by the saturation state (Ω_{CaCO_3}). As a result of the decrease in

seawater Ω_{CaCO_3} and despite the different correlations, Ω_{CaCO_3} exhibits calcification at different ecosystem levels and time scales (Andersson & Gledhill, 2013; Langdon & Atkinson, 2005; Langdon et al., 2000). Thermodynamic changes in these carbonate species ($[\text{H}^+]$, Ω_{CaCO_3}) are expected to slow the formation (and/or make it more energetically demanding) of skeletal and shell structures comprising calcium carbonate minerals (Cohen et al., 2009; Kleypas et al., 1999).

While the dynamics and trends in carbonate chemistry are reasonably well understood for open ocean waters, how anthropogenic ocean acidification (OA) unfolds within coastal zones is less understood. Many coastal regions already experience low surface seawater pH and Ω_{CaCO_3} conditions (“localized or coastal OA”) due to processes other than CO_2 uptake (Cyronak et al., 2014; Duarte et al., 2013). Observations from 20 years of carbonate data collected at a coastal station in Bermuda show that dissolved inorganic carbon (DIC) and the aragonite saturation state (Ω_{arag}) have changed at a rate of 2 to 3 times faster than the offshore Bermuda Atlantic Time series Study (BATS) station (Bates, 2017). Time series observations at fixed sites (Bates et al., 2012; Gruber et al., 2002; Sutton et al., 2017; Sutton, Sabine, Maenner-Jones, et al., 2014) have been critical for documenting these small variations and the long-term chemical changes in the surface of the open ocean. However, only a few records of at least two of the four parameters needed to resolve the carbonate system are presently available due to the significant effort and expense involved in maintaining such time series (Bates et al., 2012; Sutton et al., 2019). Another major challenge for monitoring coastal acidification is that the time series requires robust data at a high frequency (subdaily) to constrain the carbonate chemistry and calibration routines, which include regular discrete measurements to assess and validate the carbonate numerical models. The coastal OA trend may take years to decades to emerge through the natural variability in some systems (Sutton et al., 2019) due to the higher frequency and higher magnitude of biological and physical processes.

Open ocean dynamics in carbonate chemistry are reasonably well constrained and can be characterized based on seawater total alkalinity (TA)-salinity and CO_2 partial pressure ($p\text{CO}_{2\text{sw}}$)-temperature relationships (Gledhill et al., 2008; Lee et al., 2006; Wanninkhof et al., 2007). However, the natural variability in nearshore environments due to benthic and coastal processes and their proximity to human coastal activities invalidate these relationships and complicate efforts to constrain anthropogenic CO_2 uptake using temporal changes in DIC. Nearshore processes, such as the upwelling of low pH waters (Feely et al., 2008), deposition of atmospheric nitrogen and sulfur (Doney et al., 2007), discharge of riverine waters (Salisbury et al., 2008), inputs of nutrients and organic matter that stimulate intense respiration and generation of CO_2 (Cai et al., 2011; Cyronak et al., 2014) or photosynthetic uptake of DIC (Manzello et al., 2012; Yeakel et al., 2015), and reef hydrodynamics (Lowe & Falter, 2015), act together to enhance or diminish the OA effects over different spatial and temporal scales. Laboratory-based experiments demonstrate that benthic fluxes exert significant control on the carbon cycle in shallow coastal areas (Anthony et al., 2013). Different benthic processes, such as groundwater discharge (Cyronak et al., 2013), sediment fluxes (Santos et al., 2012), community (algae, sand, coral, microbial) metabolism (Kleypas et al., 2011), and organic matter remineralization (Andersson & Mackenzie, 2012), can potentially affect carbonate chemistry. However, a recent experiment in a natural coral reef environment in Bermuda (Long et al., 2019) observed that the water column contributed 58% versus the benthic contribution of 39% to organic metabolism.

The major biologically driven changes in the carbonate system (Gattuso et al., 1998) can be described by net ecosystem production ($\text{NEP} = \text{photosynthesis} - \text{respiration}$) and net ecosystem calcification ($\text{NEC} = \text{calcification} - \text{dissolution}$). The combination of NEP and NEC changes the seawater TA to DIC ratio (2:1), which in turn dictates the variability in the sea surface pH, $p\text{CO}_{2\text{sw}}$, and Ω_{CaCO_3} (Zeebe & Wolf-Gladrow, 2001). Interactions between changes in benthic community composition, water column communities, and organic carbon sources/sinks as they face stress or change over time and space are poorly understood. As a result, global projections of OA and carbonate chemistry may not be valid for coral reefs, mangroves, and estuaries, where most of the affected organisms (e.g., mussels, oysters, corals, and coralline algae) reside. The effects of OA in coastal ecosystems can be several times higher and faster than typically expected for oceanic waters (Duarte et al., 2013).

The Wider Caribbean Region (WCR, 8–28°N, 58–89°W) has experienced accelerating changes in water chemistry (Andersson et al., 2019; Gledhill et al., 2008) and sea surface temperature (SST) (Chollett et al., 2012) that could subject reef ecosystems to suboptimal conditions by the end of this century

(Hoegh-Guldberg et al., 2007). Modeling results show that over the past 20 years (from 1992 to 2015), rates of OA (based on the % change in $[H^+]$) have increased by 10%, and surface ocean Ω_{arag} has decreased by 8% in the Caribbean Sea and subtropical North Atlantic Ocean (Meléndez & Salisbury, 2017). To advance OA research in the WCR, the National Ocean Acidification Observing Network (NOA-ON) and the NOAA Pacific Marine Environmental Laboratory (PMEL, www.pmel.noaa.gov/co2) established a few efforts dedicated to monitoring the carbon cycle in environmentally sensitive and economically valuable reef systems. These sustained observations of carbonate data were used to determine site-specific algorithms for TA and pCO_{2sw} and to assess robust OA dynamics and trends over subdecadal time scales.

The Cheeca Rocks (CR) reef in the Florida Keys National Marine Sanctuary and the Enrique Cay in the Marine Reserve of La Parguera (LP), Puerto Rico, have provided 8 and 10 years, respectively, of air and seawater pCO_2 and pH, along with SST and sea surface salinity (SSS), and oxygen (O_2). These robust measurements are taken continuously at high resolution and validated with climate quality (Newton et al., 2015) discrete measurements. In this study, we characterize the seasonal variations and assess the physical and biogeochemical processes that cause different seasonal amplitudes at the two different latitudes. The results of this work will likely aid in determining the dominant processes with regard to how OA unfolds within coastal reef areas.

2. Materials and Methods

2.1. Study Sites

The La Parguera Marine Reserve is in a well-developed insular shelf that extends 10–11 km from the coast and consists of different habitat types dominated by seagrasses, macroalgal beds, unconsolidated carbonate sediments, and mangroves (Figure 1). The area is minimally affected by coastal development. The local environmental and anthropogenic stressors include bleaching, coral reef infectious diseases, and fishing (García-Sais et al., 2008). The absence of local rivers combined with very low regional rainfall and coastal runoff corresponds to minimal local freshwater inputs (Pittman et al., 2010). However, there is a seasonal freshwater influx associated with the regional river plumes of the Amazon and Orinoco Rivers (Corredor & Morell, 2001). The buoy is located 2.5 km from the southwest coast of Puerto Rico (17.95°N, 67.05°W) on the forereef of the Enrique middle-shelf reef at 3-m depth (Figure 1). McGillis et al. (2011) noted an approximately 10% live coral coverage area during belt transect surveys at the site in March 2009. These data agree with the 10–11% live coral coverage data collected in August 2015 and June 2017 (Manzello, Enochs, Kolodziej, et al., 2018; Manzello et al., 2017). A survey conducted in 2011 by Moyer et al. (2012) showed no seasonal variation in the benthic cover of the noncalcifying algae (cyanobacteria, macroalgae, and turf algae). However, Pittman et al. (2010) reported a peak of turf algae and macroalgal cover in summer. Moyer et al. (2012) found no significant seasonal changes in benthic calcifiers when the octocorals (soft coral) were excluded.

The upper Florida Keys (Figure 1) consist of a bank-barrier coral reef system, where a noncontinuous offshore barrier reef is situated parallel to the islands of the Florida Keys at approximately 7–10 km from land (Ginsburg & Shinn, 1964). Between the barrier reef and the islands lies the Hawk Channel. This area consists primarily of shallow (<8 m) seagrass and sand, with occasional, isolated patch reefs intermixed (Jones, 1977). The CR is an isolated, nearshore patch reef, approximately 2.5 km off the coast of Islamorada. The buoy (24.90°N, 80.62°W) is in 3–4 m of water. The CR is affected by shoreline development, which can impair water quality due to stormwater runoff and sewage effluent (Somerfield et al., 2008). The warm waters of the Florida Current and episodes of cold-water outflow from Florida Bay produce larger water temperature ranges in the inshore reefs of the upper Keys (Banks et al., 2007; Manzello et al., 2012). Hurricanes and tropical storms, thermal stress, and disease outbreaks can affect benthic communities during the summer and fall at both reefs (Precht & Miller, 2007). The percent coral cover in the Caribbean, including CR and LP, has declined over the past three decades due to coral bleaching and disease as well as hurricanes, corallivorous mollusks, poor water quality, and overfishing (Ballantine et al., 2008; Gardner et al., 2003; Hughes, 1994; Morelock et al., 2001). The die-off of the long-spined sea urchin *Diadema antillarum* limited coral recovery and prevented recruitment to bare substrates due to the increased algae cover (Ballantine et al., 2008; Jaap et al., 2008).

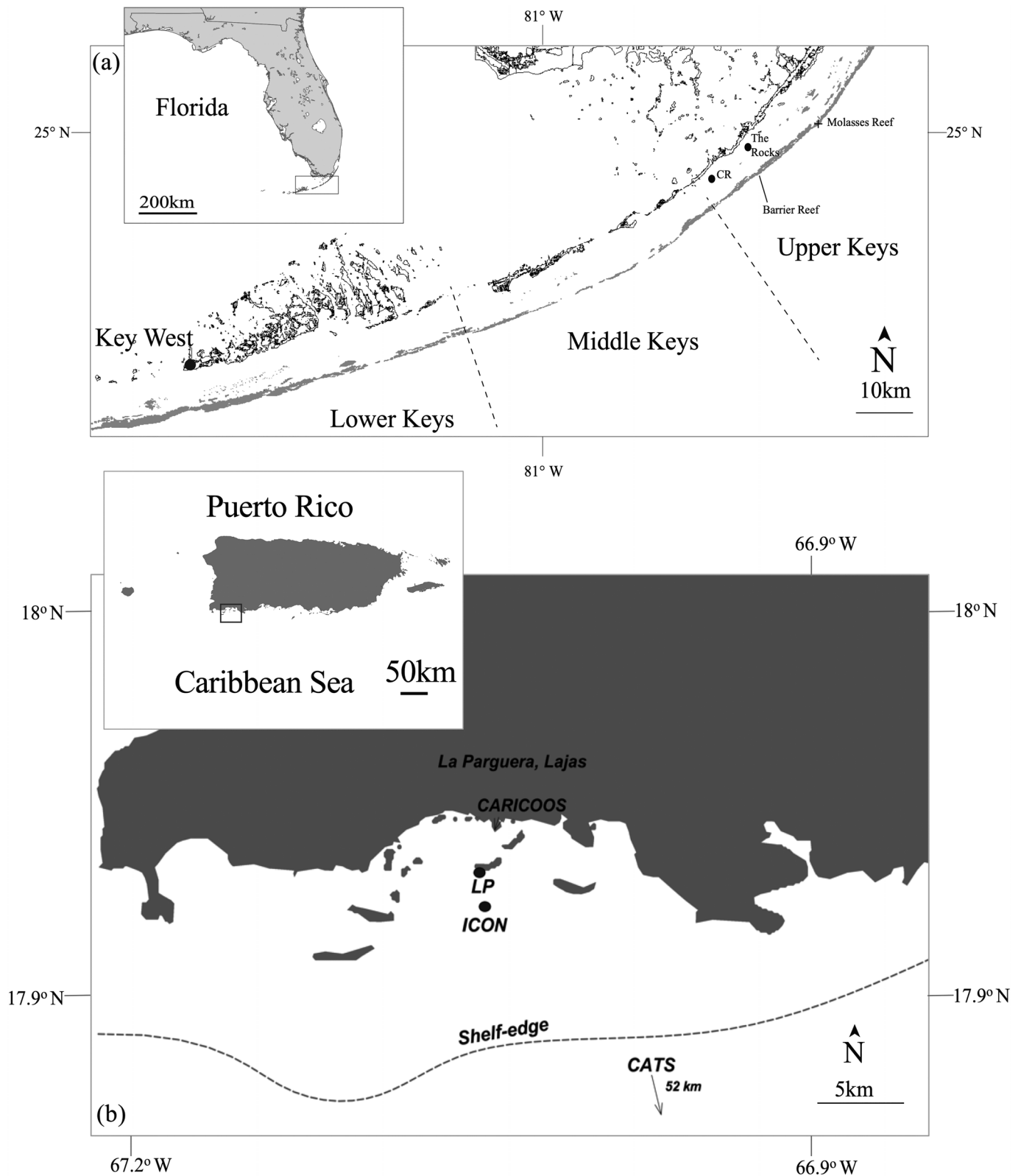


Figure 1. (a) Map of the Florida Keys and Florida Reef Track. The Cheeca Rocks (CR) MapCO₂ buoy (24.90°N, 80.62°W), the Rocks (24.94°N, -80.55°W), and the Molasses Reef Light (25.01°N, 80.38°W) stations are in the Upper Keys and marked with black circles. (b) Map showing the town of La Parguera, Lajas (18.05°N, 67.05°W), which is located southwest of the coast of Puerto Rico. The La Parguera (LP) MapCO₂ buoy (17.95°N, 67.05°W) and the ICON station (17.94°N, 67.05°W) are marked with black circles. The CARICOOS meteorological station (17.97°N, -67.04°W) is on Magueyes Island. The Caribbean Time Series station (CaTS, 17.36°N, 67°W) is 52 km south (seaward) of the shelf edge (dashed black line).

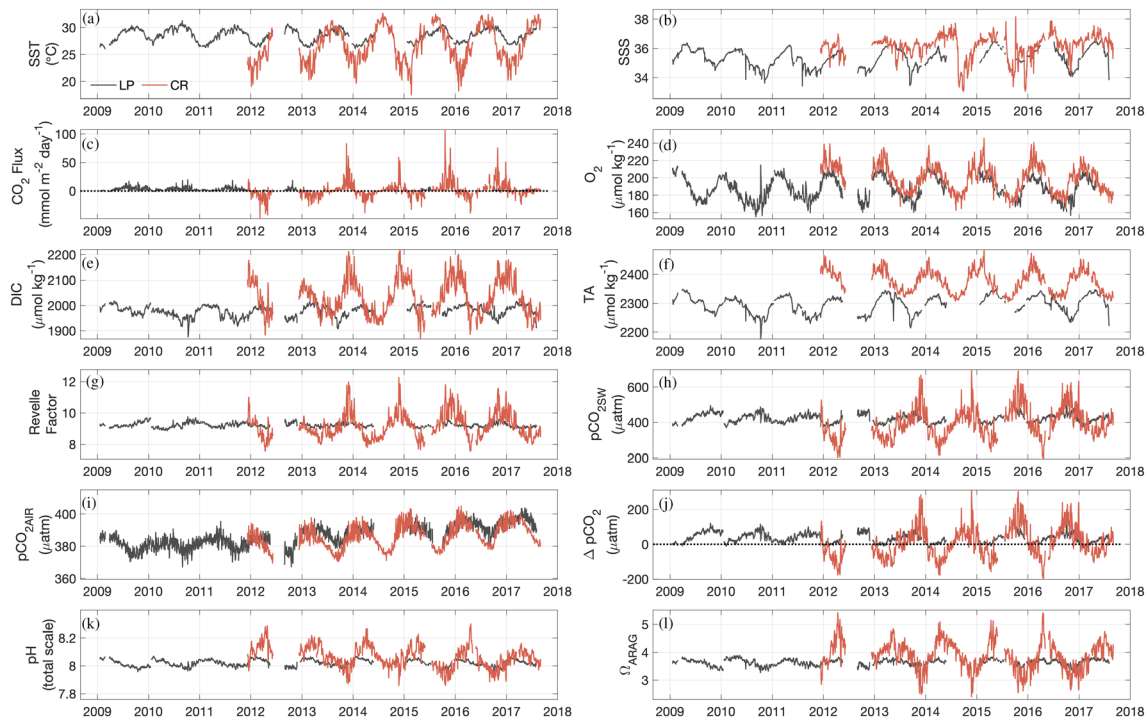


Figure 2. Multiannual time series oceanography and carbonate chemistry parameters at La Parguera (black) and Cheeca Rocks (red) from January 2009 and December 2011 to September 2017. Daily averaged sea surface in situ and derived observations of (a) temperature (SST; °C), (b) salinity (SSS), (c) CO₂ flux (mmol m⁻² day⁻¹), (d) postcorrected oxygen from the MAX-250+ sensor (O₂; μmol kg⁻¹), (e) derived dissolved inorganic carbon (DIC; μmol kg⁻¹), (f) derived total alkalinity (TA; μmol kg⁻¹), (g) derived Revelle factor, (h) seawater pCO₂ (pCO_{2sw}; μatm), (i) boundary layer atmospheric (pCO_{2air}; μatm), (j) air-sea gradient of pCO₂ (ΔpCO₂; μatm), (k) derived pH (total scale), and (l) derived aragonite saturation state (Ω_{arag}). The derived carbonate parameters are functions of pCO_{2sw} and TA. The derived TA is a function of SST and SSS (Equation 1).

2.2. Observations

2.2.1. Autonomous Observation Capabilities

Both time series (Figure 2) are ongoing projects supported by the NOAA Coral Reef Conservation Program (CRCP), which were established in January 2009 (LP) and December 2011 (CR). These test beds have since been adopted as long-term sustained monitoring stations providing physical, chemical, and ecological data under the National Coral Reef Monitoring Program (NCRMP) jointly sponsored by NOAA CRCP and the NOAA Ocean Acidification Program (OAP). Details about the efforts supporting these time series stations are described in supporting information Text S1.

The capability of LP- and CR-moored autonomous pCO₂ (MapCO₂) buoys provides continuous 3-hr measurements of both CO_{2air} and CO_{2sw} mole fractions (xCO_{2air} and xCO_{2sw}). These are converted to pCO₂ with total uncertainties of <1 and <2 μatm, respectively (Sutton, Sabine, Maenner-Jones, et al., 2014). The buoys are equipped with a seawater-gas equilibrators, reference gas standard, an infrared gas analyzer, Seabird (SBE16 or SBE37) conductivity and temperature recorders, and a Sunburst™ SAMI-pH system located at approximately 1-m depth. Details of the MapCO₂ instrument calibration and data quality assurance and quality control (QA/QC) processes are described in Sutton, Sabine, Maenner-Jones, et al. (2014) and Sutton, Sabine, Feely, et al. (2016). Measurements used for the analyses cover from January 2009 and December 2011 to September 2017 for LP and CR, respectively (Sutton, Sabine, Manzello, et al., 2016; Sutton, Sabine, Morell, et al., 2014).

The MapCO₂ buoys also include an Aanderaa™ oxygen optode (Aanderaa 4775, accuracy of ±5%) and an ECO FLNTU (WETLabs, Inc.), which are used to determine chlorophyll fluorescence and turbidity. These sensors can be used to track biological variability and abundance in the water column. In addition, the buoys have an internal Maxtec™ oxygen sensor (MAX-250+) located inside the CO₂ electronics tube (downstream from the infrared gas analyzer sensor) to measure the percent of oxygen in the air (% O₂, ±3%). The seawater surface oxygen concentration (μmol kg⁻¹) can be calculated from the MAX-250+ using the oxygen solubility

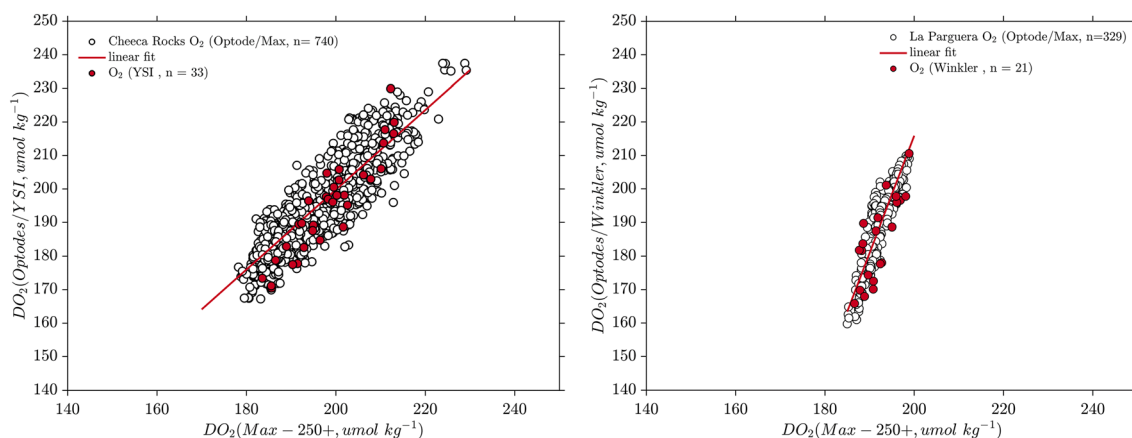


Figure 3. Linear correlation between MAX-250+ and Optode (white dots) and Winkler/YSI dissolved oxygen (DO_2) observations (red dots) for CR (a) and LP (b). The coefficients (slope \pm standard error) used to correct the MAX-250+ sensor at CR and LP were 1.19 ± 0.02 and 3.11 ± 0.05 , and the applied offsets (intercept \pm standard error) were -37.90 ± 4.76 and -475 ± 15 , respectively.

(Garcia & Gordon, 1992) as a function of in situ seawater temperature and salinity. Details about the oxygen optode QA/QC process and the MAX-250+ postcorrection are described in supporting information Text S2 and Figure S1.

The linear correlation (r^2) between MAX-250+ and the optodes was high (0.84 and 0.80), and root mean square errors (RMSEs) were small (5 and $7 \mu\text{mol kg}^{-1}$) for LP and CR, respectively. The corrected MAX-250+ oxygen observations show a significant linear correlation ($p < 0.0001$) with the optodes and discrete measurements. The linear correlation between MAX-250+ and Winkler/YSI was 0.60 and 0.85, and the RMSE was 8 and $7 \mu\text{mol kg}^{-1}$ for LP and CR, respectively. The mean differences in oxygen concentration between the YSI/Winkler and MAX-250+ were 3.3 and $7.1 \mu\text{mol kg}^{-1}$, respectively. We corrected the MAX-250+ oxygen measurements using the slope and offset of the linear correlation with the optodes (Figure 3).

Hourly wind measurements from 2006 to 2013 were taken from the nearby NOAA Integrated Coral Observing Network (ICON) station (17.94°N , 67.05°W), located 1.8 km south of the LP buoy (Hendee, 2014). Wind data from 2015 to 2017 were taken from the Caribbean Coastal Ocean Observing System (CARICOOS) meteorological station (17.97°N , 67.04°W) located 1.5 km north of the buoy. Wind speeds from the ICON and CARICOOS stations were measured at 6.5- and 7.8-m heights, respectively. Wind data gaps were filled using a climatological curve created with these two data sets. The nearest wind data available for the CR were obtained from the Molasses Reef Light location (25.01°N 80.38°W), located 27 km north of the buoy. The wind speed at this station was measured at a height of 15.8 m. These methods were preferred over the use of buoys far from the study sites or satellite wind measurements, as their use tends to overestimate the gas air-sea exchange due to their low temporal coverage and limited nearshore spatial coverage (Jiang et al., 2008). Wind speeds at both stations were normalized to the 10-m-height wind speed (Hsu et al., 1994) and averaged daily.

2.2.2. Discrete Geochemical Surveys

High-quality discrete measurements of TA, DIC, and pH were taken weekly and biweekly between 8 a.m. and 12 p.m. (LP) and 1 to 4 p.m. (CR) to validate and supplement the autonomous observations (Manzello, Enochs, & Dutra, 2018; Manzello et al., 2015, 2017; Meléndez et al., 2019). Details about the collection, analyses, intervals of available discrete data, and TA and DIC analysis precision are described in supporting information Text S3 and Figure S2. Limitations on the temporal resolution of these discrete measurements prevent the capture of diel cycles (details are discussed in section 3.1).

Discrete TA and DIC samples from seasonal cruises around the Caribbean and Atlantic Region were used to determine the mean TA and DIC oceanic conditions. No seasonal variations were observed, and we assumed that changes in TA and DIC were consistent from year to year. Details about these cruises are described in supporting information Text S4. The DIC and TA measurements were normalized by the mean oceanic salinity ($S = 36$) using Friis (2003) to correct for the influence of freshwater addition and removal.

2.3. Modeling—First-Order Derivations of TA and Calculation of Carbonic Acid System

The TA algorithms from discrete TA measurements showed a moderate correlation with seawater salinity and temperature ($r^2_{LP} = 0.55$; $r^2_{CR} = 0.41$), with RMSE values of 30 and 45 $\mu\text{mol kg}^{-1}$ for LP and CR, respectively. Nevertheless, we find that the relationships are highly significant ($p < 0.0001$; $n_{LP} = 547$; $n_{CR} = 100$). The resultant multivariate linear relationship for TA_{LP} and TA_{CR} is described as follows:

$$TA_{LP} = 43.2 (\pm 0.08) \times SSS - 12.5 (\pm 0.07) \times SST + 1,118.1 (\pm 2.10) \quad (1)$$

$$TA_{CR} = 2.2 (\pm 0.25) \times SSS - 11.8 (\pm 0.04) \times SST + 2,612.7 (\pm 9.1) \quad (2)$$

where (\pm) is the standard error of the coefficients. The reef CO_2 -carbonic acid system was fully solved using modeled TA (Equations 1 and 2) and the buoy's $p\text{CO}_{2\text{sw}}$, salinity, and temperature measurements at 1 decibar (pressure at 1 m). The MATLAB program CO2SYS (van Heuven et al., 2011) was used to determine the carbonate chemistry parameters. We applied the dissociation constants for K_1 and K_2 of Lueker et al. (2000) and $K_{\text{HSO}_4^-}$ from Dickson (1990).

We intended to describe when and where it is most difficult to precipitate CaCO_3 and the seasonal magnitude of the physiochemical constraint based on the observed Ω_{arag} values. The abiotic precipitation of CaCO_3 is thermodynamically favored ($\Omega > 1$) when the ratio of the concentration product of carbonate [CO_3^{2-}] and [Ca^{2+}] is greater than the stoichiometric solubility product (K^*_{SP}). When the ratio is less than K^*_{SP} , chemical dissolution is favored ($\Omega < 1$), and if they are in equilibrium ($\Omega = 1$), no net dissolution or precipitation is expected. The solubility constant used to derive Ω_{arag} is from Mucci (1983).

Model uncertainties for Ω_{arag} , DIC, oxygen, and CO_2 fluxes considered errors associated with the estimation of TA and $p\text{CO}_{2\text{sw}}$ as well as errors in the dissociation constants, instrument sampling, laboratory analyses, and model coefficients. We used Monte Carlo simulations and the new MATLAB function *error* by Orr et al. (2018). Details about the error analyses are described in supporting information Text S5.

2.4. Air-Sea Exchange

The applied transfer velocity-wind speed relationship is described by Wanninkhof (2014).

The air-sea CO_2 flux (F_{CO_2}) is estimated as follows:

$$F_{\text{CO}_2} = ks \times (p\text{CO}_{2\text{sw}} - p\text{CO}_{2\text{air}}) \quad (3)$$

where $p\text{CO}_{2\text{sw}} - p\text{CO}_{2\text{air}}$ is the air-sea gradient in $p\text{CO}_2$ ($\Delta p\text{CO}_2$; μatm), s ($\text{mol kg}^{-1} \text{atm}^{-1}$) is the solubility of CO_2 per unit volume of seawater (Weiss, 1974), and k (m s^{-1}) is the transfer velocity as a function of wind speed at 10 m above mean sea level.

2.5. Annual Climatology

We use the average daily observations to construct the annual climatology for each parameter and derive products to examine the seasonal cycles. The composite year is constructed by binning the data within the representative Julian day. Both time series are compiled into four distinct seasons: winter (January–March), spring (April–June), summer (July–September), and fall (October–December). The seasonal variability was computed using the peak-to-peak amplitude. The statistical significance of the seasonal amplitudes was evaluated using Student's t -tests at 0.01 and 0.05 significance levels after a normality check (supporting information Text S5).

The buoy of LP was replaced in 2014, which produced the highest number of missing observations. Other gaps in the time series occurred intermittently due to instrument failure and buoy annual servicing. Although the measurements are occasionally unavailable, all seasons were sampled at both time series. Details about the time series gaps and intervals of available data are described in supporting information Text S6, Table S1, and Figure S3.

2.6. Spatiotemporal Integration of the $p\text{CO}_{2\text{sw}}$ and Discrete TA and DIC Observations

In an effort to better understand the predominant spatial extent over which the buoy measurements are integrated and the physical forcing that controls the residence times and accumulation of the chemical signature

from biogeochemical processes in these shallow reefs (Lowe & Falter, 2015), near-reef currents were assessed using acoustic Doppler current profilers (ADCPs) and a tilt current meter (TCM). Details of these deployments are described in supporting information Text S7. These physical observations provide a more comprehensive interpretation of how to infer local biogeochemical processes given the autonomous $p\text{CO}_{2\text{sw}}$ and oxygen measurements respond on much shorter spatiotemporal scales than the discrete DIC and TA (Takeshita et al., 2018).

Residence times at LP and CR were measured using the inputs and outputs of Beryllium-7 (Venti et al., 2012, 2014) to assess how TA and DIC discrete samples are integrated over temporal and spatial scales. We assumed that the biogeochemical processes modify the carbonate chemistry as the water mass flows over the shelf platform from the open ocean end-member. Based on these results (see text below for details), discrete TA and DIC measurements represent metabolic processes that have been integrated over multiple days and spatial scales greater than 10 km, while the $p\text{CO}_{2\text{sw}}$ and oxygen chemical signatures represent processes on diel timescales (hours) by the communities close (<5 km) to the buoy. Based on the physicochemical characteristics (e.g., currents, winds, residence times, and salinity changes) at both locations, we assume that variability associated with larger-scale oceanic processes occurs at time scales much longer than the reef's spatiotemporal scales.

Polar histograms of current speed, direction, and frequency were used to characterize the dominant currents at the sites (Figures S4 and S5). At LP, the dominant current at ADCP W (west) was 1.24 cm s^{-1} (1.1 km day^{-1}) toward the west-northwest and $280\text{--}290^\circ$ from true north (Figure S6). This result is in good agreement with the results observed by McGillis et al. (2011). The ADCP W shows low seasonal variation and was situated almost precisely upstream from the buoy, which allows for a robust estimation of the residence time between the buoy and the forereef. Taking the distance between the ADCP W and the buoy as 0.18 km and a dominant current of 1.24 cm s^{-1} , the water that reaches the buoy at LP traverses over the forereef for at least 4 hr. The current histogram (Figure S7) presented for ADCP E (east) shows a dominant current of 1.72 cm s^{-1} (1.5 km day^{-1}) directed toward the southwest in good alignment with the east-end orientation of the forereef, which suggests that currents at this site predominantly follow the reef morphology. It is likely that the actual time the water has been in contact with the Enrique forereef is longer than the above calculation. If we assume the water reaching the buoy traversed along the forereef from ADCP E to ADCP W, as suggested by the dominant currents presented in the histograms, then the residence time of the water exposed to reef conditions could be up to 16 hr. Over a semidiurnal cycle (12 hr), the spatial scale of these measurements is approximately 0.5 km. Residence times from Beryllium-7 between the buoy site and 11 km offshore (17.87°N , -67.02°W) were measured in 2011. These results indicate that the shelf platform processes are integrated over 9 and 11 ± 2 days. These time scales agree with the current speed measured by the ADCPs.

The TCM deployment at CR showed a dominant current mean speed of 7.98 cm s^{-1} (7 km day^{-1}) toward the southwest at 222° with no seasonal variation (Figure S8). According to the ocean current results, the water reaching the reef was previously north of the buoy (Figure S5). Over a semidiurnal cycle, the spatial scale of the measurements represents biogeochemical and thermodynamic processes from 3 km north of the buoy. Then the buoy data from CR represent water that is about to contact the reef. The buoy's chemistry may reflect processes from areas north of the buoy, primary composed of seagrass, macroalgae, fine-grained CaCO_3 sediments and rocks, and some isolated hard and soft corals. Seagrass communities upstream of the buoy at CR can produce high-frequency variability in the carbonate chemistry on diel timescales, which can contribute to the greater variability observed at CR relative to that at LP. The Beryllium-7 average residence time between the offshore and inner reef areas in the upper Florida Keys is estimated to be 5.6 ± 1.7 days with no significant seasonal variation (Muehllehner et al., 2016).

3. Results and Discussion

3.1. Model Versus In Situ Observations and Carbonate Uncertainties

The statistical results from the linear correlations between the discrete and modeled/buoy measurements are presented in supporting information Table S2 (see also Figure S9 for a graphical representation of the seasonal modeled and discrete data). The average difference between the $p\text{CO}_{2\text{sw}}$ buoy measurements and $p\text{CO}_{2\text{sw}}$ calculated from discrete measurements was $<1 \mu\text{atm}$. The average difference between the

SAMI-pH and spectrophotometric pH measurements at LP was 0.01, and the difference between the derived pH (from discrete TA and DIC) and SAMI-pH at CR was 0.005. The modeled and discrete TA differences over the annual mean were 2 and 0.3 $\mu\text{mol kg}^{-1}$ for LP and CR, respectively. The CO2SYS modeling program (Orr et al., 2018) was used to numerically characterize the uncertainties produced from modeled TA and $p\text{CO}_{2\text{sw}}$ for the carbonate chemistry calculations (Figure S10). The uncertainties in the calculated $[\text{CO}_3^{2-}]$ for LP and CR are 2% and 4%, respectively. This result is close to the *climate* goal (<1%) needed to identify decadal trends (Newton et al., 2015). The final carbonate uncertainties are summarized in Table S3. This data comparability, achieved with widely differing methods, demonstrates the robust quality of our analytical procedures and resulting data.

Uncertainties in our derived parameters (DIC, Ω_{arag} , pH, and Revelle factor) are mostly associated with the TA linear model at both sites. These uncertainties arise primarily from calcification and dissolution. Collecting TA during the day may result in biases toward daytime processes, although it may partially represent the diurnal variability around the “true” TA mean. For example, several studies have shown that TA varied over a diurnal cycle by as much as $70 \pm 24 \mu\text{mol kg}^{-1}$ in the Florida coral reefs (Turk et al., 2015) and ranged from 4 to 31 $\mu\text{mol kg}^{-1}$ at LP (McGillis et al., 2009). The use of seasonal modeled TA values may reduce the potential biases caused by diurnal processes.

3.2. Seasonal Variability in Carbonate Chemistry

Mean conditions and seasonal amplitudes from the annual climatology (Figure 4) in measured and modeled parameters are presented in Table 1. On an annual scale, CR experiences greater seasonal amplitude in seawater temperature than LP. This difference is primarily due to the larger magnitude in regional air temperatures and net atmospheric heat flux. At CR, the seawater temperature seasonal variation was 6°C greater and the mean summer conditions were 1°C to 2°C warmer compared with the reef at LP. Although conditions during the summertime at CR were warmer than those at LP, throughout most of the annual year (67%), the temperatures were from 5°C to 6°C cooler than those at LP. The elevated temperatures (>30°C) between August and October coincided with low salinities at both stations. Both sites experienced similar seawater salinity seasonal patterns and varied annually by 2. The seasonal summer evaporation and local rainfall during the fall further affect the salinity changes at both sites. Year round, the salinity at LP was 1.2 to 1.6 units fresher than that at CR, with a maximum difference from October to January. The resulting difference may be due to the significant role that the Orinoco and Amazon River plumes play in freshening the system between May and October in the eastern Caribbean region (Corredor & Morell, 2001; Fournier et al., 2017; Salisbury et al., 2011).

The DIC and TA at LP showed similar salinity seasonal patterns. These seasonal cycles were associated with cooling and lower DIC and TA pools from the freshwater influx of regional river plumes during the fall (Cai et al., 2010; Cooley, 2006). The seasonal DIC and TA amplitudes (60 and 89 $\mu\text{mol kg}^{-1}$) were smaller relative to CR (221 and 117 $\mu\text{mol kg}^{-1}$). The seasonal amplitudes of DIC and TA were significant ($p < 0.01$) despite the model errors (Table S3) for both sites. At a typical seawater pH of 8.02, the significant contributions of phosphorus and silicate concentrations to TA and DIC (>1 $\mu\text{mol kg}^{-1}$) were at concentrations >1 and >30 $\mu\text{mol kg}^{-1}$, respectively. The relatively low concentrations of these inorganic nutrients (<1 $\mu\text{mol kg}^{-1}$) and the potential contribution to TA and DIC at both stations were nonsignificant (<0.01%) and therefore neglected (see supporting information Text S7 and Figure S11 for more details).

The seasonal amplitudes in the modeled and discrete normalized TA and DIC (nTA and nDIC) at CR were approximately 180 and 300 $\mu\text{mol kg}^{-1}$, respectively (Figure S12). At CR, the nDIC and nTA increased from August to January and decreased from February to June. We observed a significant consumption ($p < 0.05$) and excess ($p < 0.05$) of discrete nTA and nDIC relative to oceanic values at CR, indicating a significant contribution from calcification/dissolution and photosynthesis/respiration processes (Figure S12). No significant ($p > 0.05$) excess of nTA relative to the oceanic mean was observed at LP. The seasonal fluctuations at LP in discrete nTA and nDIC were 37.5 and 43 $\mu\text{mol kg}^{-1}$, respectively. The nDIC and nTA at LP increased from June to December and decreased from January to May. Although the seasonal variations are less pronounced at LP, the seasonal amplitudes of the modeled and discrete nTA and nDIC were statistically significant ($p < 0.05$). Changes in nTA and nDIC due to biogeochemical processes are evaluated separately in section 3.3.1.

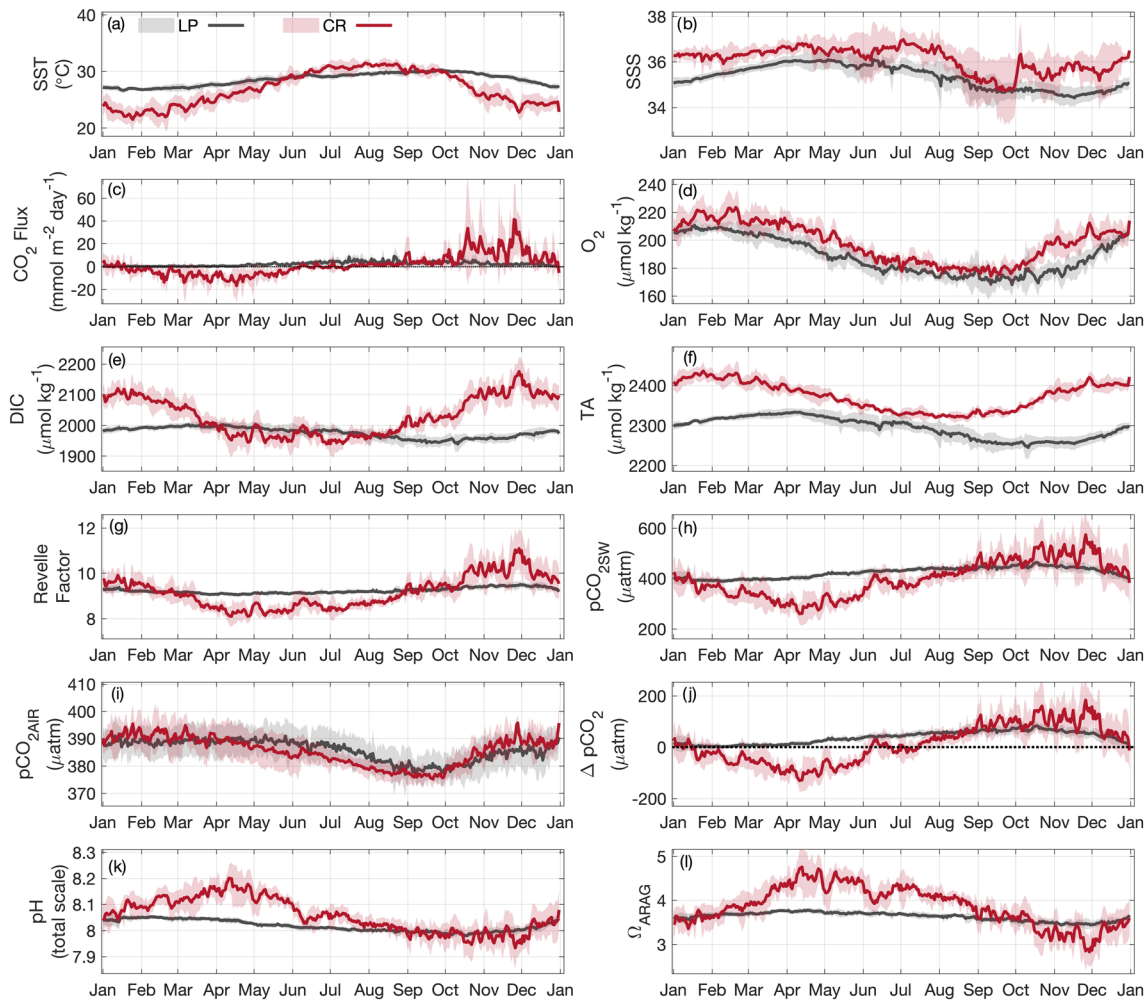


Figure 4. Seasonal patterns for the period from January 2009 to September 2017 (LP, black) and from December 2011 to September 2017 (CR, red). The black and red lines represent the composite year mean values, and the gray and red shading indicate the standard deviation of each measurement. Seasonal climatologies of (a) temperature (SST; °C), (b) salinity (SSS), (c) CO₂ flux ($\text{mmol m}^{-2} \text{day}^{-1}$), (d) postcorrected oxygen from the MAX-250+ sensor (O_2 ; $\mu\text{mol kg}^{-1}$), (e) derived dissolved inorganic carbon (DIC; $\mu\text{mol kg}^{-1}$), (f) derived total alkalinity (TA; $\mu\text{mol kg}^{-1}$), (g) Revelle factor, (h) seawater $p\text{CO}_2$ ($p\text{CO}_{2\text{sw}}$; μatm), (i) boundary layer atmospheric ($p\text{CO}_{2\text{air}}$; μatm), (j) air-sea gradient of $p\text{CO}_2$ ($\Delta p\text{CO}_2$; μatm), (k) derived pH (total scale), and (l) derived aragonite saturation state (Ω_{arag}). The derived carbonate parameters are functions of $p\text{CO}_{2\text{sw}}$ and TA. The derived TA is a function of SST and SSS (Equation 1).

The net annual exports of carbon from the water to the atmosphere at LP and CR were $+0.88 \pm 0.66$ and $+0.56 \pm 3.37 \text{ mol CO}_2 \text{ m}^{-2} \text{ year}^{-1}$, respectively. These fluxes are relatively weak when compared with other reef locations, such as Bermuda (Bates et al., 2001) and Kaneohe Bay, Hawaii (Fagan & Mackenzie, 2007; Massaro et al., 2012). This difference can be related to different factors, including the method used, meteorological and physicochemical characteristics, $p\text{CO}_{2\text{sw}}$ temperature sensitivity, and biological processes. On an annual basis, the Enrique forereef was a persistent source of CO₂ to the atmosphere ($+2.41 \pm 1.80 \text{ mmol CO}_2 \text{ m}^{-2} \text{ day}^{-1}$, $p < 0.05$). The F_{CO_2} seasonal amplitude was approximately $+9 \text{ mmol CO}_2 \text{ m}^{-2} \text{ day}^{-1}$, with a minimum of $0.08 \text{ mmol CO}_2 \text{ m}^{-2} \text{ day}^{-1}$ in February and a maximum of $+8.89 \text{ mmol CO}_2 \text{ m}^{-2} \text{ day}^{-1}$ in August. Conversely, the F_{CO_2} at CR ranged from -16.64 to $+41.41 \text{ mmol CO}_2 \text{ m}^{-2} \text{ day}^{-1}$. From January to June (43% of the annual year), the CR reef was a net sink for CO₂. This finding is consistent with previous results found in Olsen et al. (2004) and Wanninkhof et al. (2007), where the northern Caribbean areas are a sink during the springtime while the southern areas remain a source of CO₂ to the atmosphere. At CR, the wind speed ranged from 3 to 9 m s^{-1} , and the prevailing wind direction was from the east, northeast, and southeast. The average daily wind speeds at LP ranged from 2 to 6 m s^{-1} and showed little seasonal

Table 1
Summary of the LP and CR Seasonal Variability in Carbonate and Oceanography Parameters

Parameter	LP (January 2009 to September 2017)		CR (December 2011 to September 2017)	
	Mean \pm SD	Seasonal amplitude	Mean \pm SD	Seasonal amplitude
Temperature ($^{\circ}\text{C}$)	28.55 \pm 1.09	3.61	26.97 \pm 3.00	9.95
Salinity	35.33 \pm 0.52	1.64	36.12 \pm 0.51	2.15
Wind speed (m s^{-1})	4.20 \pm 0.74	4.01	5.58 \pm 1.36	6.46
O_2 ($\mu\text{mol kg}^{-1}$)	191.41 \pm 11.79	39.39	197.92 \pm 13.73	47.98
DIC ($\mu\text{mol kg}^{-1}_{\text{sw}}$)	1,977.28 \pm 16.36	60.48	2,029.29 \pm 60.22	221.85
TA ($\mu\text{mol kg}^{-1}_{\text{sw}}$)	2,295.2 \pm 26.49	88.77	2,372.57 \pm 35.47	117.39
nDIC ($\mu\text{mol kg}^{-1}_{\text{sw}}$)	2,009.6 \pm 14.33	47.91	2,030.3 \pm 59.04	218.08
nTA ($\mu\text{mol kg}^{-1}_{\text{sw}}$)	2,334.6 \pm 13.06	42.61	2,370.4 \pm 35.44	124.61
Revelle factor	9.26 \pm 0.11	0.43	9.14 \pm 0.65	2.78
$p\text{CO}_{2\text{sw}}$ (μatm)	425.76 \pm 21.61	73.71	397.30 \pm 69.10	284.25
$p\text{CO}_{2\text{air}}$ (μatm)	386.26 \pm 3.28	13.82	384.41 \pm 6.06	22.68
$\Delta p\text{CO}_{2\text{sea-air}}$ (μatm)	38.51 \pm 24.40	81.88	12.90 \pm 72.43	285.61
pH (total scale)	8.02 \pm 0.02	0.07	8.06 \pm 0.06	0.25
Ω_{arag}	3.62 \pm 0.09	0.33	3.87 \pm 0.43	1.80
F_{CO_2} ($\text{mmol m}^{-2} \text{day}^{-1}$)	2.05 \pm 1.44	6.71	1.48 \pm 8.57	51.82

Note. The mean conditions and standard deviation (\pm) are from the daily averaged observations. The seasonal amplitudes were calculated using the peak-to-peak change from the composite annual year.

variation. The prevailing wind directions were from the east and southeast. The $\Delta p\text{CO}_{2\text{sea-air}}$ and F_{CO_2} seasonal patterns were similar at both sites, suggesting that wind speed plays a smaller role than thermodynamic and biological changes.

The $p\text{CO}_{2\text{air}}$ fluctuations were modest at CR and LP (24 and 13 μatm) and similar to the reported regional $\text{CO}_{2\text{air}}$ values (see supporting information Text S8 for more details). Maximum seawater $p\text{CO}_{2\text{sw}}$ values in LP were observed from August through October, while the minima occurred during the wintertime when the surface $p\text{CO}_{2\text{sw}}$ decreased to nearly the atmospheric equilibrium ($\sim 390 \mu\text{atm}$). The $p\text{CO}_{2\text{sw}}$ seasonal amplitude in LP was minor (73 μatm) relative to the significant annual change (284 μatm) experienced in CR. The seawater $p\text{CO}_{2\text{sw}}$ in CR fluctuated between 100 and 175 $\mu\text{atm day}^{-1}$ during the fall, where the annual maximum values were $544 \pm 69 \mu\text{atm}$ (Figure 4). In the spring, the $p\text{CO}_{2\text{sw}}$ decreased to a minimum of $260 \pm 69 \mu\text{atm}$. This corresponded to an oversaturation of $p\text{CO}_{2\text{sw}}$ by 140% and an undersaturation of 65% from the annual mean atmospheric value ($384 \pm 6.1 \mu\text{atm}$).

The pH and Ω_{arag} seasonal patterns were similar at both sites, with minimum values from October to November and maximum values from February to April, respectively. The pH amplitude at LP was small (0.07) relative to CR (0.25). The mean pH conditions (based on $[\text{H}^+]$) during the fall in LP and CR were 15% and 44% lower (“more acidic”), respectively, relative to the wintertime. The Ω_{arag} in CR was 38% higher in spring than in fall and winter and ranged from 4.73 (April) to 2.93 (November). At LP, the Ω_{arag} seasonal amplitude was 0.3, with a maximum of 3.78 ± 0.09 (April) and a minimum of 3.44 ± 0.09 (November). The mean Ω_{arag} at LP was 3.63 ± 0.09 and 3.87 ± 0.44 at CR. The Ω_{arag} values at both locations systematically decreased from summer to fall despite the increase in temperature and the thermodynamic effect on mineral solubility. These results agreed with previously calculated seasonal fluctuations for LP and CR (Manzello, Enochs, Kolodziej, et al., 2018; Manzello et al., 2012; Sutton, Sabine, Manzello, et al., 2016).

The mean buffer capacity at both stations showed similar seasonal patterns, albeit differing amplitudes. The Revelle factor in CR ranged from 8.10 to 10.87 from spring to fall. In contrast, the Revelle factor at LP only fluctuated from 9.06 to 9.49. The oxygen seasonal pattern was comparable at both sites, with a minimum during summer and fall when the $p\text{CO}_{2\text{sw}}$ was at the maximum value. The oxygen seasonal cycles were supported by three in situ independent measurements using calibrated optical oxygen sonde and Winkler oxygen discrete measurements, calibrated Aanderaa optodes, and MAX-250+ sensors (Figure S1). At both sites, the increase in $p\text{CO}_{2\text{sw}}$ and the decrease in oxygen and pH from summer to fall suggested that organic biological processes involving CO_2 production play an important role in modifying pH and Ω_{arag} .

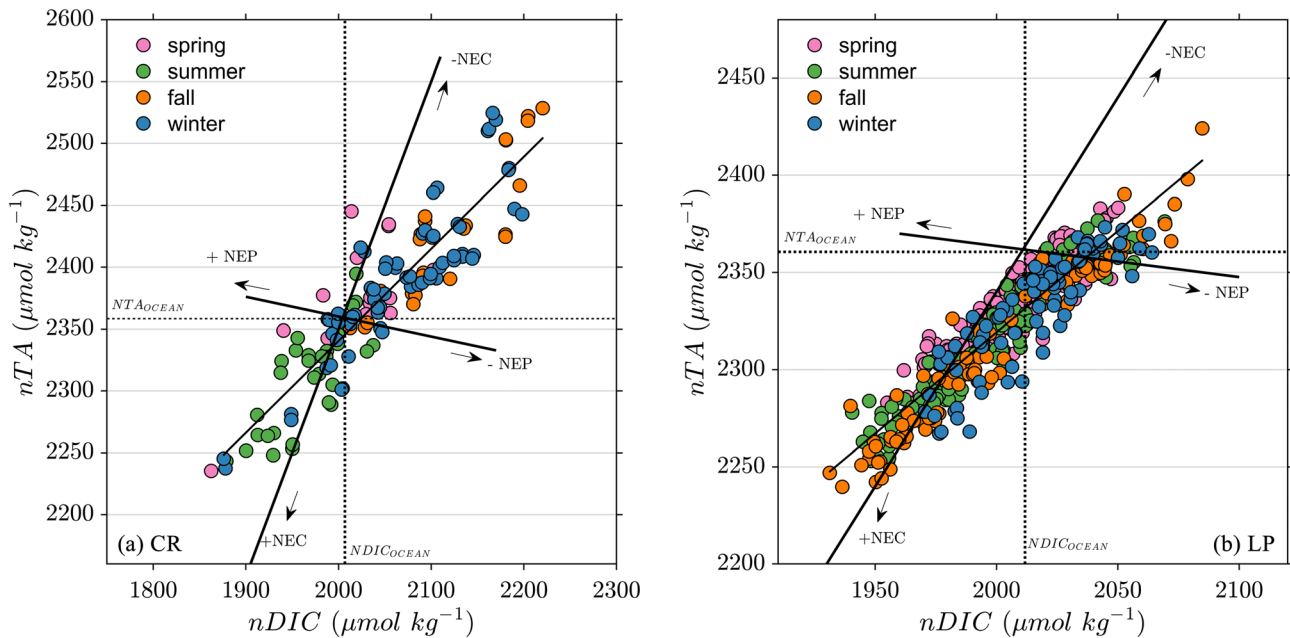


Figure 5. Relationship between salinity-normalized DIC ($nDIC$; $\mu\text{mol kg}^{-1}$) and TA (nTA ; $\mu\text{mol kg}^{-1}$) using the discrete measurements collected at LP ($n = 499$) and CR ($n = 141$). Measurements were normalized by the mean oceanic salinity ($S = 36.0$). The average ocean nTA and $nDIC$ values are denoted by gray dashed lines. The pink (spring), green (summer), orange (fall), and blue (winter) colors represent the different seasons. The line TA to DIC slopes expected from NEC and NEP are in solid black lines.

3.3. Relative Contributions of Organic and Inorganic Carbon Processes to Seasonal Variability

3.3.1. Changes in Discrete nTA and $nDIC$ Concentrations

The $nTA:nDIC$ slopes can be used to describe changes in biogeochemical processes (Deffeyes, 1965; Lantz et al., 2014). For example, net calcification increases $nTA:nDIC$ slopes (>1), while net production decreases the $nTA:nDIC$ slopes. We assume that processes such as nutrient uptake/release and ammonia and sulfate reduction have minor effects in these two coral reef ecosystems relative to the influence of net calcification and productivity. These processes should be carefully considered in ecosystems where nutrient and organic acid concentrations are high (Andersson & Mackenzie, 2012; Dickson, 2010). We assumed that the discrete measurements are representative of daytime processes; however, sampling schemes that can capture biological diel cycles and respond to changes in water residence time and mixed tidal cycles are needed in subsequent studies. Note that biogeochemical processes from DIC and TA observations likely respond to much longer spatiotemporal scales than the pCO_{2sw} and oxygen measurements (see section 2.6 for more details).

The $nTA:nDIC$ slopes observed at CR and LP were 0.74 ± 0.03 and 1.0 ± 0.02 , respectively. These results were in accordance with the results of Cyronak et al. (2018) and consistent with patterns observed in other reef areas with longer integration times. This finding suggests that reef metabolism at both locations modulates nearshore water chemistry relative to the oceanic mean conditions. The relative influence of organic metabolism on DIC was higher at CR (63%) than at LP (50%), following Equation 1 as detailed in Cyronak et al. (2018), suggesting that productivity plays a more important role in driving chemical variability at CR. It is possible that this difference is because metabolic processes at CR are integrated over the platform for shorter residence times (days) than at LP (days to weeks). According to Takeshita et al. (2018), net calcification becomes more critical than net production when integrated over multiple days (i.e., net production is balanced, but calcification is always positive over a diurnal cycle).

Figure 5 shows that most of the data points at CR fall into the lower left and upper right quadrants, indicating that calcification and dissolution could play an important role in the seasonal carbonate dynamics. Prior work described in the Florida Keys has associated the changes in nTA and $nDIC$ with net calcification (Muehllehner et al., 2016) and benthic primary productivity (Manzello et al., 2012). The seasonal chlorophyll cycle (Figure S11), determined from measurements taken at the nearby station (Rocks) from 1995 to 2014,

shows low values throughout the year ($<0.5 \mu\text{g L}^{-1}$) with a slight increase from February to April ($>1 \mu\text{g L}^{-1}$), supporting the hypothesis of an increase in photosynthesis during spring.

While calcification is an important process throughout much of the year at LP, respiration appears to provide an additional source of DIC to the system, particularly during the fall. We hypothesize that calcification within the reef-shelf platform reduces TA relative to that of offshore communities. Interestingly, the data cluster at LP does not pass through the ocean nTA and nDIC intercept. With limited ship-based data in the Caribbean region, this discrepancy is likely due to the poor characterization of the ocean end-member. Careful consideration should be taken when calculating or interpreting biogeochemical processes using the anomaly technique or the graphical analysis of TA and DIC vectors at LP.

3.3.2. Changes in O_2 and $p\text{CO}_{2\text{sw}}$ Buoy Observations

To further explore the relative contributions of biological processes in carbonate chemistry seasonal changes, we used autonomous $p\text{CO}_{2\text{sw}}$ and oxygen measurements (Joesoef et al., 2015; Shadwick et al., 2011; Takahashi et al., 2002). Note that these high-frequency buoy observations fill the temporal uncertainties in the discrete nTA and nDIC, integrate the diurnal activity over longer time scales, and provide information about processes at an ecosystem scale.

The seasonal variations in $p\text{CO}_{2\text{sw}}$ are caused by the interaction among thermodynamics, physical processes (e.g., air-sea exchange and mixing), and biological processes. The correlation between logarithm of $p\text{CO}_{2\text{sw}}$ and temperature shows no apparent linear correlation ($r^2 = 0.05$) and a deviation (i.e., 0.012°C^{-1}) from the $p\text{CO}_{2\text{sw}}$ dependence with temperature ($0.0423^\circ\text{C}^{-1}$) estimated by Takahashi et al. (1993). This finding suggests that the temperature effects on $p\text{CO}_{2\text{sw}}$ at CR are offset by biological productivity, air-sea exchange, and mixing. At LP, $p\text{CO}_{2\text{sw}}$ shows a significant ($r^2 = 0.60$; $p < 0.01$) linear correlation with temperature, and the slope is similar ($0.0409^\circ\text{C}^{-1}$) to the $p\text{CO}_{2\text{sw}}$ temperature dependence of Takahashi et al. (1993). This result suggests that at LP, thermodynamics were dominant with little biological compensation to offset the temperature $p\text{CO}_{2\text{sw}}$ sensitivity. To normalize the $p\text{CO}_{2\text{sw}}$ ($np\text{CO}_{2\text{sw}}$) and explore the relative contribution of biology (assuming that the effects of physical transport are small) on the $p\text{CO}_{2\text{sw}}$ seasonal changes, we used the thermodynamic coefficient estimated by Takahashi et al. (1993) at a mean temperature of 28.6°C and 26.9°C for LP and CR, respectively.

The observed changes in oxygen likely reflect variations in biology at both sites. Higher residence times at LP may enhance the magnitude of the chemical signals relative to CR. However, seagrass beds such as those north of CR may offer greater potential to change oxygen, while at LP, no significant seagrass beds are found upstream of the buoy. The use of apparent oxygen utilization (AOU) removes the solubility effects of oxygen, which are primarily driven by temperature changes. We assume that AOU changes are much less affected by physical processes, such as ventilation, air-sea exchange, and lateral export. Then oxygen consumption by respiration is closely related to AOU greater than zero, and oxygen production by photosynthesis is related to AOU lower than zero. The AOU seasonal patterns are supported by independent oxygen measurements (Figure S1) and regional patterns on chlorophyll (Figures S11 and S13).

A simulation using the temperature normalization of $p\text{CO}_{2\text{sw}}$ to consider the fraction of the air-sea gradient of $p\text{CO}_2$ ($\Delta p\text{CO}_{2\text{sea-air}}$) that is caused by biological ($\Delta p\text{CO}_{2\text{bio}}$) versus thermal ($\Delta p\text{CO}_{2\text{temp}}$) processes was performed (Takahashi et al., 2002). This result was qualitatively compared with the AOU observations to consider the organic carbon dynamics. For example, if $\Delta p\text{CO}_{2\text{bio}}$ is below or near zero (or constant) during heterotrophic conditions, then biological processes that decrease $p\text{CO}_{2\text{sw}}$ (i.e., dissolution) are dominant.

At LP, the biological processes affecting the $p\text{CO}_2$ air-sea gradient were relatively constant, except for a small increase from mid-September to mid-December (Figure 6). Heterotrophic conditions dominated from mid-spring to fall, and autotrophic conditions dominated from December to mid-April at LP. Although McGillis et al. (2009, 2011) do not provide seasonal data and the integrated daily rates of net metabolism at Enrique's forereef are variable, our results agree with the time of the year when they obtained measurements. Given our assumptions, the dissolution processes under heterotrophic conditions maintained a constant $\Delta p\text{CO}_{2\text{bio}}$. Gray et al. (2012) found that respiration and dissolution are dominant at a nearby reef (north of Enrique) from summer to fall. Note that the lowest annual Ω_{arag} and pH values were observed during the same time of the year (Figure 4). The AOU decreased from November to December, and $\Delta p\text{CO}_{2\text{bio}}$ values increased, suggesting an increase in calcification or a decrease in dissolution. During autotrophic

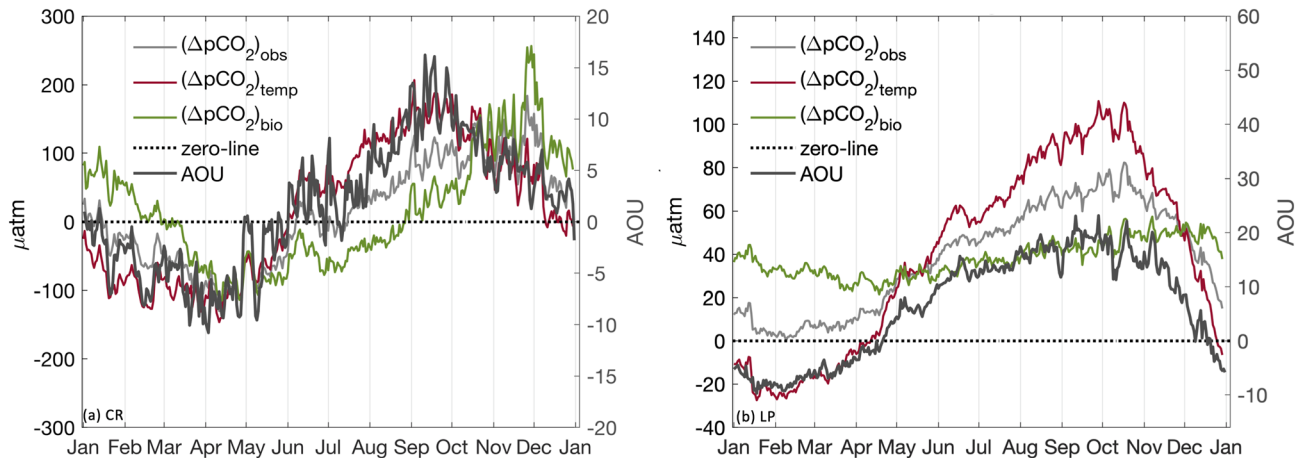


Figure 6. Seasonal biological ($\Delta p\text{CO}_{2\text{bio}}$, green line) and thermal ($\Delta p\text{CO}_{2\text{temp}}$, red line) effects on observed $\Delta p\text{CO}_{2\text{sea-air}}$ ($\Delta p\text{CO}_{2\text{obs}}$, gray line) for CR (a) and LP (b). The apparent oxygen utilization (AOU) is represented with a black line on the second axis.

conditions, we hypothesize that calcification keeps $\Delta p\text{CO}_{2\text{bio}}$ relatively constant. Low biological productivity (and high respiration) caused the Enrique foreereef to serve as a net source of CO₂ to the atmosphere year round.

At CR, heterotrophic conditions were observed from June to mid-September; $\Delta p\text{CO}_{2\text{bio}}$ was below zero, suggesting dissolution or a decrease in calcification. From mid-September to the end of May, the AOU systematically decreased, and a positive biological affecting the $p\text{CO}_{2}$ air-sea gradient suggested calcification, which produced a transition from a net sink to a net source of CO₂ to the atmosphere. It is reasonable to consider that respiration and dissolution co-occur or that they are closely related in this work based on prior work described elsewhere (Gattuso et al., 1999) and in the Florida Keys at seasonal (Muehllehner et al., 2016) and diurnal (Turk et al., 2015) time scales. For example, Muehllehner et al. (2016) showed that photosynthesis and calcification dominate in April, May, and August and respiration and dissolution dominate in October and December.

3.4. Seasonal Hysteresis Between the Carbonate Chemistry and Biological Activity

The response lag in the water column chemistry, as either a driver or a reflection of reef metabolism, can contribute to the seasonal hysteresis (Cyronak et al., 2013; Jokiel et al., 2014; McMahan et al., 2013; Shamberger et al., 2011). However, separating biogeochemical processes from water column measurements is difficult because the reef and water column are not mutually exclusive, resulting in a dynamic interaction (Andersson & Gledhill, 2013). While several studies have shown the presence of hysteresis at diurnal time scales, seasonal hysteresis that link biological processes to environmental conditions remains elusive, partially because of the lack of high-frequency and long-term measurements in nearshore areas. We described the seasonal hysteresis between metabolic processes and seawater chemistry (temperature and Ω_{arag}) using two biological indices ($np\text{CO}_{2\text{sw}}$ and AOU).

The feedback between biological processes and the reef seawater chemistry shows an elliptical relation at both stations (Figures 7 and 8). Figure 7 shows the CR and LP $np\text{CO}_{2\text{sw}}$ seasonal results plotted versus the in situ temperature and are colored by the Ω_{arag} seasonal values. Figure 7 shows that the difference in the magnitude of hysteresis between both locations is large because of the seasonal temperature variations and the effects of biological processes on $p\text{CO}_{2\text{sw}}$ and seawater carbonate chemistry. Interestingly, the magnitude of the AOU (horizontal component or broader aspect of the ellipsoid) is similar at both sites (Figure 8). The seasonal strength (shape or magnitude) of the hysteresis is linked to the effect of benthic metabolism on the water chemistry (Jokiel et al., 2014). Several hypotheses for the mechanisms of the observed seasonal hysteresis between seawater carbonate chemistry and biological metabolism include seasonal changes in benthic communities (e.g., seagrasses and corals), environmental switches (e.g., nutrients and carbon availability), and stressful abiotic conditions (e.g., temperature and pH). Changes in ecosystem processes at seasonal time scales, including coral-algal competition and even hurricanes and bleaching, can also produce

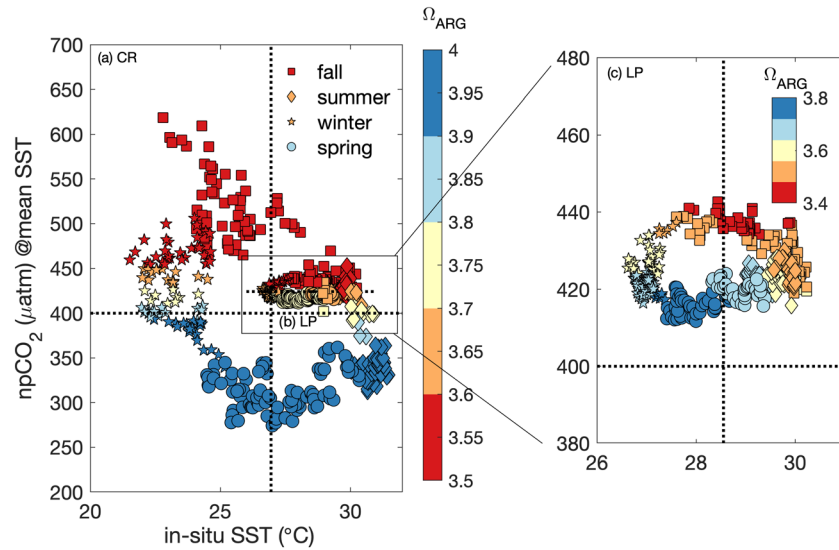


Figure 7. Seasonal hysteresis of temperature-normalized $p\text{CO}_{2\text{sw}}$ ($\text{npCO}_{2\text{sw}}$; μatm) relative to in situ temperature ($^{\circ}\text{C}$) and colored by Ω_{arag} for CR (a) and LP (b). Panel (c) shows a magnified view of LP. The square (fall), diamond (summer), star (winter), and circle (spring) symbols represent the different seasons. The seasonal means of SST and $p\text{CO}_{2\text{air}}$ ($400 \mu\text{atm}$) are denoted by the gray dashed lines.

significant alterations in the ecosystem and different hysteresis loops (Knowlton, 1992; Petraitis & Hoffman, 2010).

At CR, the results show that lower $\text{npCO}_{2\text{sw}}$ (greater than the seasonal mean $p\text{CO}_{2\text{air}}$) values are from winter to early summer, with higher temperatures (less than the seasonal mean temperature) from spring to August (Figure 7). During spring, the $\text{npCO}_{2\text{sw}}$ values decreased to $250 \mu\text{atm}$ (sink conditions), and Ω_{arag} was at the

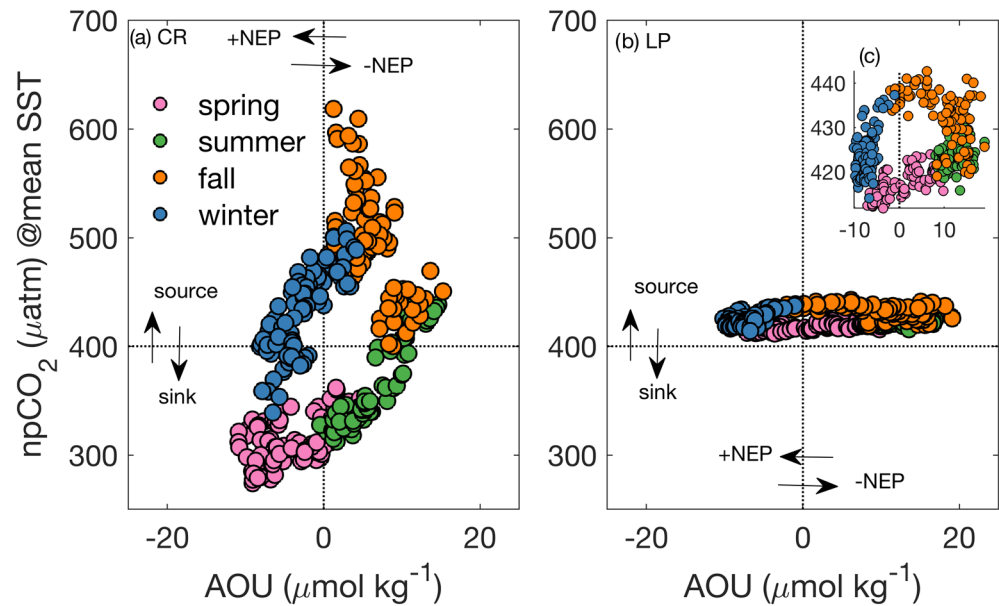


Figure 8. Temperature-normalized $p\text{CO}_{2\text{sw}}$ ($\text{npCO}_{2\text{sw}}$; μatm) and the apparent oxygen utilization (AOU; $\mu\text{mol kg}^{-1}$) for CR (a) and LP (b), where the pink (spring), green (summer), orange (fall), and blue (winter) colors represent the different seasons. Panel (c) shows a magnified view of LP. The $p\text{CO}_{2\text{air}}$ mean of $400 \mu\text{atm}$ is denoted by the horizontal gray dashed line. AOU values greater than zero (vertical gray dashed line) denote heterotrophic (respiration $>$ photosynthesis) and less than zero autotrophic (respiration $<$ photosynthesis) conditions.

highest values, ranging from 3.8 to 4 (Figures 7 and 8). These low $npCO_{2sw}$ conditions support the observations of Manzello et al. (2012), where uptake of CO_2 by the spring seagrass and macroalgae bloom increases biological production and significantly increases Ω_{arag} at time scales longer than diurnal. Consistent with the Coral Reef Ecosystem Feedback hypothesis (CREF, Bates et al., 2009), an increase in net productivity stimulates increasing Ω_{arag} by reducing $[H^+]$ and CO_2 . During late summer and fall, the $npCO_{2sw}$ increased above the atmospheric annual mean of 400 to $>600 \mu atm$ and the Ω_{arag} ranged from 3.5 to 3.7 (Figures 7 and 8). Net heterotrophic and lower Ω_{arag} conditions can be linked to an increase in respiration during a postbloom by the same primary producers upstream of CR. The unidirectional southward water current observed in this study (Figure S8) supports the hypothesis that the outflow from upstream waters affects water chemistry downstream.

At LP, the hysteresis between seawater chemistry and biological activity was muted relative to that at CR (Figures 7 and 8). The results at LP showed year-round high $npCO_{2sw}$ values with no seasonal shifts (Figures 7 and 8). The seasonal $npCO_{2sw}$ versus temperature relationship follows an ellipsoid with higher Ω_{arag} at lower $npCO_{2sw}$ values (Figure 7). The increase in respiration (Figure 8) decreases pH, and the salinity-driven decreases in $[CO_3^{2-}]$ and $[Ca^{2+}]$ drive down Ω_{arag} during the fall (Gledhill et al., 2010; Gray et al., 2012; Moyer et al., 2012). Moyer et al. (2012) found that the reef's ability to modify water chemistry is low at LP because (1) the benthic community dominated by soft corals continued to increase despite the decrease in Ω_{arag} , (2) no significant primary producers (i.e., seagrass beds) are found upstream, and (3) the absence of fast-growing branching corals (i.e., *Acropora* sp.) and low live coral cover ($<10\%$). Although reef metabolism may not be a significant factor in changing seawater carbonate chemistry at LP, we observed that high Ω_{arag} and low $npCO_{2sw}$ correspond to autotrophic conditions (Figures 7 and 8).

The seasonal feedback between benthic metabolism and seawater carbonate chemistry at LP is weakened relative to that at CR and other Atlantic high-latitude reefs (Bates et al., 2009), which shows that autotrophic conditions in early summer increase Ω_{arag} and coral calcification. We hypothesize that Ω_{arag} is suppressed from spring to fall because of substantial contributions from organic matter respiration attributed to mangrove-derived organic matter inputs as well as by allochthonous carbon sources (e.g., Yeakel et al., 2015). Although calcification was not measured in this study, we hypothesize that summer net calcification in the shelf platform reduces the open ocean source water TA significantly as indicated by the discrete nTA measurements (Figure 5). Therefore, upstream communities could decrease Ω_{arag} and make calcification more energetically demanding in the mid-shelf and inshore reefs. We hypothesize that longer residence times and shallowness at this site could favor enhanced chemical signal (e.g., pCO_{2sw}) from dark respiration and calcification (Anthony et al., 2011; Takeshita, 2017; Takeshita et al., 2018). Long residence times can also increase the accumulation of TA flux from the dissolution of carbonate sediments and the coral framework. Still, because the TA model is derived from salinity and temperature, it cannot adequately capture alkalinity variations from calcification and dissolution.

4. Conclusions

We found dissimilar effects of temperature and biology on carbonate chemistry at the two locations whereby the seasonal cycle at CR was amplified relative to LP. Temperature effects on pCO_{2sw} at CR were largely counteracted by biological productivity, while at LP, carbonate chemistry dynamics were driven primarily by thermodynamics. The resulting CO_2 fluxes show LP as a persistent source of CO_2 to the atmosphere, while CR transitioned from net source to net sink of CO_2 from fall to spring. The biological processes from the seagrass communities close to the CR buoy enhanced the carbonate chemistry over diurnal and seasonal scales relative to LP despite the longer residence times observed at LP. We found evidence suggesting that from late summer to fall, respiration and dissolution are the dominant biogeochemical processes at both locations. During the same time in the annual cycle, increases in DIC from respiration and a decrease in salinity from regional freshwater sources (at LP) decrease Ω_{arag} despite the temperature effect on mineral solubility at both places. We observed that autotrophic conditions from winter to early spring could provide favorable conditions for calcification by increasing Ω_{arag} while substantial contributions from organic carbon can make calcification more energetically demanding during the fall. Uncertainties exist in the coastal organic matter inputs from local (from seagrasses or mangroves) and remote sources, particularly the regional freshwater sources impinging in the eastern Caribbean during fall. Simple linear trends cannot explain

the feedback between metabolism and reef water chemistry using long-term observations over natural variations. The effects of community production on $p\text{CO}_{2\text{sw}}$ make these interactions complex at short- and long-term scales. The seasonal response between benthic metabolism and seawater chemistry at LP is attenuated relative to that at CR because of their differences in benthic cover and how benthic metabolism modifies the water chemistry at this location.

The discrete nTA and nDIC dynamics show that while calcification is an important process throughout much of the year at LP (summer at CR), respiration, particularly in late summer and fall, appears to be an important source of additional CO_2 to the systems. At LP, calcification from the outer shelf communities and inputs of organic matter from mangroves likely reduce Ω_{arag} and increase the susceptibility of inshore reefs to OA effects. However, changes in discrete nTA and nDIC reflect biological activity that has been integrated over multiple days at the shelf scale (>10 km), while the buoy measures $p\text{CO}_{2\text{sw}}$ dynamics on diel timescales by the communities upstream of the buoy (<5 km). Careful consideration should be taken when inferring local biogeochemical processes, given that $p\text{CO}_{2\text{sw}}$ (and presumably pH) responds on much shorter time and local scales than DIC and TA at the studied locations. Our observations highlight the need for more comprehensive observing systems that can reliably measure both the fast-response ($p\text{CO}_{2\text{sw}}$ and pH) and slow-response (DIC) carbon pools. This study provided valuable indices that can be used by coastal managers and industry leaders in their decision making in the face of OA and warming.

Data Availability Statement

Data supporting this research are available in these in-text data citation references: J. Corredor (1994), Hendee (2014), Manzello et al. (2015, 2017), Manzello, Enochs, and Dutra (2018), Meléndez et al. (2019), Sutton, Sabine, Morell, et al. (2014), and Sutton, Sabine, Manzello, et al. (2016). Data products related to the paper are temporarily included as supporting information and will be available upon publication in the respective Integrated Ocean Observing System (IOOS) regional associations (CARICOOS and SECORA) repositories, as well to the NCEI data repository. Wind data for the station IMGP4 – Isla Magueyes, Lajas, Puerto Rico, can be found at https://www.ndbc.noaa.gov/station_page.php?station=IMGP4 and for the Station MLRF1 – Molasses Reef, Florida at https://www.ndbc.noaa.gov/station_page.php?station=MLRF1. The data from the Rocks station are part of the Southeast Environmental Research Center Florida International University (SERC-FIU) Water Quality Monitoring Network. USA EPA Agreement #X7 00D02412-1 and NOAA Agreement #NA09NOS4260253 and can be found at <http://serc.fiu.edu/wqmnetwork/FKNMS-CD/DataDL.htm>. UPRM participation in the latter is made possible through the IOOS partnership with CARICOOS program.

References

- Andersson, A. J., & Gledhill, D. (2013). Ocean acidification and coral reefs: Effects on breakdown, dissolution, and net ecosystem calcification. *Annual Review of Marine Science*, 5(1), 321–348. <https://doi.org/10.1146/annurev-marine-121211-172241>
- Andersson, A. J., & Mackenzie, F. T. (2012). Revisiting four scientific debates in ocean acidification research. *Biogeosciences*, 9(3), 893–905. <https://doi.org/10.5194/bg-9-893-2012>
- Andersson, A. J., Venn, A. A., Pendleton, L., Brathwaite, A., Camp, E. F., Cooley, S., et al. (2019). Ecological and socioeconomic strategies to sustain Caribbean coral reefs in a high- CO_2 world. *Regional Studies in Marine Science*, 29, 100677. <https://doi.org/10.1016/j.rsma.2019.100677>
- Anthony, K. R. N., Diaz-Pulido, G., Verlinden, N., Tilbrook, B., & Andersson, A. J. (2013). Benthic buffers and boosters of ocean acidification on coral reefs. *Biogeosciences*, 10(7), 4897–4909. <https://doi.org/10.5194/bg-10-4897-2013>
- Anthony, K. R. N., Kleypas, A., & Gattuso, J. P. (2011). Coral reefs modify their seawater carbon chemistry—Implications for impacts of ocean acidification. *Global Change Biology*, 17(12), 3655–3666. <https://doi.org/10.1111/j.1365-2486.2011.02510.x>
- Ballantine, D. L., Appeldoorn, R. S., Yoshioka, P., Weil, E., Armstrong, R., Garcia, J. R., et al. (2008). Biology and ecology of Puerto Rican coral reefs. In *Coral reefs of the USA* (pp. 375–406). Dordrecht: Springer. https://doi.org/10.1007/978-1-4020-6847-8_9
- Banks, K. W., Riegl, B. M., Shinn, E. A., Piller, W. E., & Dodge, R. E. (2007). Geomorphology of the southeast Florida continental reef tract (Miami-Dade, Broward, and Palm Beach counties, USA). *Coral Reefs*, 26(3), 617–633. <https://doi.org/10.1007/s00338-007-0231-0>
- Bates, N. R. (2017). Twenty years of marine carbon cycle observations at Devils Hole Bermuda provide insights into seasonal hypoxia, coral reef calcification, and ocean acidification. *Frontiers in Marine Science*, 4, 1–23. <https://doi.org/10.3389/fmars.2017.00036>
- Bates, N. R., Amat, A., & Andersson, A. J. (2009). The interaction of ocean acidification and carbonate chemistry on coral reef calcification: Evaluating the carbonate chemistry Coral Reef Ecosystem Feedback (CREF) hypothesis on the Bermuda coral reef. *Biogeosciences Discussions*, 6(4), 7627–7672. <https://doi.org/10.5194/bgd-6-7627-2009>
- Bates, N. R., Best, M. H. P., Neely, K., Garley, R., Dickson, A. G., & Johnson, R. J. (2012). Detecting anthropogenic carbon dioxide uptake and ocean acidification in the North Atlantic Ocean. *Biogeosciences*, 9(7), 2509–2522. <https://doi.org/10.5194/bg-9-2509-2012>

Acknowledgments

Support for this study was provided by the NOAA's Coral Reef Conservation Program through its AOAT project and the Ocean Acidification Program (OAP). We would like to give special thanks to Dr. Jorge Corredor for the opportunity of working with him and his work throughout the development of the La Parguera time series. We also thank the staff and students of the UPRM Marine Sciences Department and UNH for field and lab assistance. We thank Helena Antoun, Belitza Brocco, Val Hensley, and Erick García from UPRM for the assistance provided with the field and laboratory samples. PMEL contribution number 5040.

- Bates, N. R., Samuels, L., & Merlivat, L. (2001). Biogeochemical and physical factors influencing seawater $f\text{CO}_2$ and air-sea CO_2 exchange on the Bermuda coral reef. *Limnology and Oceanography*, 46(4), 833–846. <https://doi.org/10.4319/lo.2001.46.4.0833>
- Cai, W. J., Hu, X., Huang, W. J., Jiang, L. Q., Wang, Y., Peng, T. H., & Zhang, X. (2010). Alkalinity distribution in the western North Atlantic Ocean margins. *Journal of Geophysical Research*, 115, C08014. <https://doi.org/10.1029/2009JC005482>
- Cai, W.-J., Hu, X., Huang, W. J., Murrell, M. C., Lehrter, J. C., Lohrenz, S. E., et al. (2011). Acidification of subsurface coastal waters enhanced by eutrophication. *Nature Geoscience*, 4(11), 766–770. <https://doi.org/10.1038/ngeo1297>
- Caldeira, K., & Wickett, M. E. (2003). Anthropogenic carbon and ocean pH. *Nature*, 425(6956), 365–365. <https://doi.org/10.1038/425365a>
- Chollett, I., Müller-Karger, F. E., Heron, S. F., Skirving, W., & Mumby, P. J. (2012). Seasonal and spatial heterogeneity of recent sea surface temperature trends in the Caribbean Sea and southeast Gulf of Mexico. *Marine Pollution Bulletin*, 64(5), 956–965. <https://doi.org/10.1016/j.marpolbul.2012.02.016>
- Cohen, A. L., McCorkle, D. C., De Putron, S., Gaetani, G. A., & Rose, K. A. (2009). Morphological and compositional changes in the skeletons of new coral recruits reared in acidified seawater: Insights into the biomineralization response to ocean acidification. *Geochemistry, Geophysics, Geosystems*, 10, Q07005. <https://doi.org/10.1029/2009GC002411>
- Cooley, S. R. (2006). *Dissolved inorganic carbon cycling in the offshore Amazon River plume and the western tropical North Atlantic Ocean* (Doctoral dissertation). Athens, Georgia: University of Georgia. Retrieved from ProQuest (https://getd.libs.uga.edu/pdfs/cooley_sarah_r_200608_phd.pdf)
- Corredor, J. (1994). *Caribbean time series* [dataset]. Sea-viewing Wide Field-of-view (SeaWiFS) Bio-optical Archive and Storage System (SeaBASS), National Aeronautics and Space Administration (NASA). <https://doi.org/10.5067/SeaBASS/CATS/DATA001>
- Corredor, J. E., & Morell, J. M. (2001). Seasonal variation of physical and biogeochemical features in eastern Caribbean Surface Water. *Journal of Geophysical Research*, 106(C3), 4517–4525. <https://doi.org/10.1029/2000JC000291>
- Cyronak, T., Andersson, A. J., Langdon, C., Albright, R., Bates, N. R., Caldeira, K., et al. (2018). Taking the metabolic pulse of the world's coral reefs. *PLoS ONE*, 13(1), e0190872. <https://doi.org/10.1371/journal.pone.0190872>
- Cyronak, T., Santos, I. R., McMahon, A., & Eyre, B. D. (2013). Carbon cycling hysteresis in permeable carbonate sands over a diel cycle: Implications for ocean acidification. *Limnology and Oceanography*, 58(1), 131–143. <https://doi.org/10.4319/lo.2013.58.1.0131>
- Cyronak, T., Schulz, K. G., Santos, I. R., & Eyre, B. D. (2014). Enhanced acidification of global coral reefs driven by regional biogeochemical feedbacks. *Geophysical Research Letters*, 41, 5538–5546. <https://doi.org/10.1002/2014GL060849>
- Deffeyes, K. S. (1965). Carbonate equilibria: A graphic and algebraic approach. *Limnology and Oceanography*, 10(3), 412–426. <https://doi.org/10.4319/lo.1965.10.3.0412>
- Dickson, A. G. (1990). Thermodynamics of the dissociation of boric acid in potassium chloride solutions from 273.15 to 318.15 K. *Journal of Chemical and Engineering Data*, 35(3), 253–257. <https://doi.org/10.1021/jc00061a009>
- Dickson, A. G. (2010). The carbon dioxide system in seawater: Equilibrium chemistry and measurements. *Guide to best practices for ocean acidification research and data reporting*, 1, 17–40.
- Doney, S. C., Mahowald, N., Lima, I., Feely, R. A., Mackenzie, F. T., Lamarque, J.-F., & Rasch, P. J. (2007). Impact of anthropogenic atmospheric nitrogen and sulfur deposition on ocean acidification and the inorganic carbon system. *Proceedings of the National Academy of Sciences*, 104(37), 14,580–14,585. <https://doi.org/10.1073/pnas.0702218104>
- Duarte, C. M., Hendriks, I. E., Moore, T. S., Olsen, Y. S., Steckbauer, A., Ramajo, L., et al. (2013). Is ocean acidification an open-ocean syndrome? Understanding anthropogenic impacts on seawater pH. *Estuaries and Coasts*, 36, 221–236. <https://doi.org/10.1007/s12237-013-9594-3>
- Fagan, K. E., & Mackenzie, F. T. (2007). Air–sea CO_2 exchange in a subtropical estuarine-coral reef system, Kaneohe Bay, Oahu, Hawaii. *Marine Chemistry*, 106(1–2), 174–191. <https://doi.org/10.1016/j.marchem.2007.01.016>
- Feely, R. A., Sabine, C. L., Hernandez-Ayon, J. M., Ianson, D., & Hales, B. (2008). Evidence for upwelling of corrosive “acidified” water onto the continental shelf. *Science*, 320(5882), 1490–1492. <http://doi.org/10.1126/science.1155676>
- Feely, R. A., Sabine, C. L., Lee, K., Berelson, W., Kleyvas, J., Fabry, V. J., & Millero, F. J. (2004). Impact of anthropogenic CO_2 on the CaCO_3 system in the oceans. *Science*, 305(5682), 362–366. <http://doi.org/10.1126/science.1097329>
- Fournier, S., Vandemark, D., Gaultier, L., Lee, T., Jonsson, B., & Gierach, M. M. (2017). Interannual variation in offshore advection of Amazon-Orinoco plume waters: Observations, forcing mechanisms, and impacts. *Journal of Geophysical Research: Oceans*, 122, 8966–8982. <https://doi.org/10.1002/2017JC013103>
- Friis, K. (2003). The salinity normalization of marine inorganic carbon chemistry data. *Geophysical Research Letters*, 30(2), 1–4. <https://doi.org/10.1029/2002GL015898>
- Garcia, H. E., & Gordon, L. I. (1992). Oxygen solubility in seawater: Better fitting equations. *Limnology and Oceanography*, 37(6), 1307–1312. <https://doi.org/10.4319/lo.1992.37.6.1307>
- García-Sais, J., Appeldoorn, R., Battista, T., Bauer, L., Bruckner, A., Caldwell, C., et al. (2008). The state of coral reef ecosystems of Puerto Rico. In J. E. Waddell & A. M. Clarke (Eds.), *The state of coral reef ecosystems of the United States and Pacific Freely Associated States*, NOAA Technical Memorandum NOS NCCOS 73 (pp. 75–116). Silver Spring, MD: NOAA/NCCOS Center for Coastal Monitoring and Assessment's Biogeography Team. Retrieved from https://coastalscience.noaa.gov/data_reports/the-state-of-coral-reef-ecosystems-of-the-united-states-and-pacific-freely-associated-states-2008/
- Gardner, T. A., Cote, I. M., Gill, J. A., Grant, A., & Watkinson, A. R. (2003). Long-term region-wide declines in Caribbean corals. *Science*, 20(516), 493–494. <https://doi.org/10.1038/020493a0>
- Gattuso, J.-P., Frankignoulle, M., & Smith, S. V. (1999). Measurement of community metabolism and significance in the coral reef CO_2 source-sink debate. *Proceedings of the National Academy of Sciences of the United States of America*, 96(23), 1,3017–1,3022. <https://doi.org/10.1073/pnas.96.23.13017>
- Gattuso, J.-P., Frankignoulle, M., & Wollast, R. (1998). Carbon and carbonate metabolism in coastal aquatic ecosystems. *Annual Review of Ecological Systems*, 29(1), 405–434. <https://doi.org/10.1146/annurev.ecolsys.29.1.405>
- Ginsburg, R. N., & Shinn, E. A. (1964). Distribution of the reef-building community in Florida and the Bahamas. *AAPG Bulletin*, 48(4), 527–527.
- Gledhill, D. K., Corredor, J. E., Langdon, C., Manzello, D., Sabine, C. L., Hensley, V., et al. (2010). Carbonate chemistry dynamics over a Caribbean shelf reef (Cayo Enrique) at the Atlantic Ocean Acidification Test-bed, La Parguera, Puerto Rico. *Amer Geophys Union*, 2010 Fall Meeting. Abstract, #OS21D-1541.
- Gledhill, D. K., Wanninkhof, R., Millero, F. J., & Eakin, M. (2008). Ocean acidification of the greater Caribbean region 1996–2006. *Journal of Geophysical Research*, 113, C10031. <https://doi.org/10.1029/2007JC004629>
- Gray, S. E. C., DeGrandpre, M. D., Langdon, C., & Corredor, J. E. (2012). Short-term and seasonal pH, $p\text{CO}_2$ and saturation state variability in a coral-reef ecosystem. *Global Biogeochemical Cycles*, 26, GB3012. <https://doi.org/10.1029/2011GB004114>

- Gruber, N., Keeling, C. D., & Bates, N. R. (2002). Interannual variability in the North Atlantic Ocean carbon sink. *Science*, 298(5602), 2374–2378. <https://doi.org/10.1126/science.1077077>
- Hendee, J. C. (2014). *US DOC/NOAA/OAR > Atlantic Oceanographic and Meteorological Laboratory. Integrated Coral Observing Network (ICON)—Media Luna Reef (LPPR1—La Parquera Natural Reserve, Puerto Rico) Meteorological and oceanographic observations from 2013-01-01 to 2013-03-20* (NCEI Accession 0124000). NOAA National Centers for Environmental Information. Retrieved from <https://accession.nodc.noaa.gov/0124000>
- Hoegh-Guldberg, O., Mumby, P. J., Hooten, A. J., Steneck, R. S., Greenfield, P., Gomez, E., et al. (2007). Coral reefs under rapid climate change and ocean acidification. *Science*, 318(5857), 1737–1742. <https://doi.org/10.1126/science.1152509>
- Hsu, S. A., Meindl, E. A., & Gilhousen, D. B. (1994). Determining the power-law wind-profile exponent under near-neutral stability conditions at sea. *Journal of Applied Meteorology*, 33(6), 757–765. [https://doi.org/10.1175/1520-0450\(1994\)033<0757:DTPLWP>2.0.CO;2](https://doi.org/10.1175/1520-0450(1994)033<0757:DTPLWP>2.0.CO;2)
- Hughes, T. P. (1994). Catastrophes, phase shifts, and large-scale degradation of a Caribbean coral reef. *Science*, 265(5178), 1547–1551. <https://doi.org/10.1126/science.265.5178.1547>
- Jaap, W. C., Szmant, A., Jaap, K., Dupont, J., Clarke, R., Somerfield, P., et al. (2008). A perspective on the biology of Florida Keys coral reefs. In *Coral reefs of the USA* (pp. 75–125). Dordrecht: Springer. https://doi.org/10.1007/978-1-4020-6847-8_3
- Jiang, L.-Q., Cai, W.-J., Wanninkhof, R., Wang, Y., & Lüger, H. (2008). Air-sea CO₂ fluxes on the U.S. South Atlantic Bight: Spatial and seasonal variability. *Journal of Geophysical Research*, C07019. <https://doi.org/10.1029/2007jc004366>
- Joesoef, A., Huang, W. J., Gao, Y., & Cai, W. J. (2015). Air–water fluxes and sources of carbon dioxide in the Delaware Estuary: Spatial and seasonal variability. *Biogeosciences*, 12(20), 6085–6101. <https://doi.org/10.5194/bg-12-6085-2015>
- Jokiel, P. L., Jury, C. P., & Ku'ulei, S. R. (2014). Coral-algae metabolism and diurnal changes in the CO₂-carbonate system of bulk sea water. *PeerJ*, 2, e378. <https://doi.org/10.7717/peerj.378>
- Jones, J. A. (1977). *Morphology and development of southeastern Florida patch reefs* (Vol. 2, pp. 231–235). Paper presented at Proceedings of the 3rd International Coral Reef Symposium.
- Kleypas, J. A., Anthony, K. R. N., & Gattuso, J. P. (2011). Coral reefs modify their seawater carbon chemistry—Case study from a barrier reef (Moorea, French Polynesia). *Global Change Biology*, 17(12), 3667–3678. <https://doi.org/10.1111/j.1365-2486.2011.02530.x>
- Kleypas, J. A., Buddemeier, R. W., Archer, D., Gattuso, J. P., Langdon, C., & Opdyke, B. N. (1999). Geochemical consequences of increased atmospheric carbon dioxide on coral reefs. *Science*, 284(5411), 118–120. <https://doi.org/10.1126/science.284.5411.118>
- Knowlton, N. (1992). Thresholds and multiple stable states in coral reef community dynamics. *Integrative and Comparative Biology*, 32(6), 674–682. <https://doi.org/10.1093/icb/32.6.674>
- Langdon, C., & Atkinson, M. J. (2005). Effect of elevated pCO₂ on photosynthesis and calcification of corals and interactions with seasonal change in temperature/irradiance and nutrient enrichment. *Journal of Geophysical Research*, 110, C09S07. <https://doi.org/10.1029/2004JC002576>
- Langdon, C., Takahashi, T., Sweeney, C., Chipman, D., Goddard, J., Marubini, F., et al. (2000). Effect of calcium carbonate saturation state on the calcification rate of an experimental coral reef. *Global Biogeochemical Cycles*, 14(2), 639–654. <https://doi.org/10.1029/1999GB001195>
- Lantz, C. A., Atkinson, M. J., Winn, C. W., & Kahng, S. E. (2014). Dissolved inorganic carbon and total alkalinity of a Hawaiian fringing reef: Chemical techniques for monitoring the effects of ocean acidification on coral reefs. *Coral Reefs*, 33(1), 105–115. <https://doi.org/10.1007/s00338-013-1082-5>
- Lee, K., Tong, L. T., Millero, F. J., Sabine, C. L., Dickson, A. G., Goyet, C., et al. (2006). Global relationships of total alkalinity with salinity and temperature in surface waters of the world's oceans. *Geophysical Research Letters*, 33, L19605. <https://doi.org/10.1029/2006GL027207>
- Long, M. H., Rheuban, J. E., McCorkle, D. C., Burdige, D. J., & Zimmerman, R. C. (2019). Closing the oxygen mass balance in shallow coastal ecosystems. *Limnology and Oceanography*, 64(6), 2694–2708. <https://doi.org/10.1002/lno.11248>
- Lowe, R. J., & Falter, J. L. (2015). Oceanic forcing of coral reefs. *Annual Review of Marine Science*, 7(1), 43–66. <https://doi.org/10.1146/annurev-marine-010814-015834>
- Lueker, T. J., Dickson, A. G., & Keeling, C. D. (2000). Ocean pCO₂ calculated from dissolved inorganic carbon, alkalinity, and equations for K₁ and K₂: Validation based on laboratory measurements of CO₂ in gas and seawater at equilibrium. *Marine Chemistry*, 70(1–3), 105–119. [https://doi.org/10.1016/S0304-4203\(00\)00022-0](https://doi.org/10.1016/S0304-4203(00)00022-0)
- Manzello, D. P., Enochs, I. C., & Dutra, E. (2018). *National Coral Reef Monitoring Program: Dissolved inorganic carbon, total alkalinity and other parameters collected from surface discrete measurements at coral reef sites in the Florida Keys, Dry Tortugas, Puerto Rico and St. Croix from 2015-12-10 to 2016-12-02* (NCEI Accession 0173496, Version 1.1). NOAA National Centers for environmental information. Retrieved from <https://doi.org/10.7289/v5t72fsd>
- Manzello, D. P., Enochs, I. C., Kolodziej, G., Carlton, R., & Valentino, L. (2018). Resilience in carbonate production despite three coral bleaching events in 5 years on an inshore patch reef in the Florida Keys. *Marine Biology*, 165(6), 99. <https://doi.org/10.1007/s00227-018-3354-7>
- Manzello, D. P., Enochs, I. C., Kolodziej, G., Carlton, R. D., & Valentino, L. M. (2015). *National Coral Reef Monitoring Program: Dissolved inorganic carbon, total alkalinity, pH and other variables collected from surface discrete observations using infrared dissolved inorganic carbon analyzer, alkalinity titrator and other instruments from the North Atlantic Ocean near Key West, Florida (Class III climate monitoring sites) from 2012-03-23 to 2014-12-11* (NCEI Accession 0132022, Version 1.1). NOAA National Centers for Environmental Information. Retrieved from <https://doi.org/10.7289/V54M92MV>
- Manzello, D. P., Enochs, I. C., Melo, N., Gledhill, D. K., & Johns, E. M. (2012). Ocean acidification refugia of the Florida Reef Tract. *PLoS one*, 7(7), e41715. <http://doi.org/10.1371/journal.pone.0041715>
- Manzello, D. P., Enochs, I. C., Valentino, L. M., Kolodziej, G., & Hendee, J. (2017). *National Oceanic and Atmospheric Administration; Cooperative Institute for Marine and Atmospheric Studies. NCRMP and OAP Class III Carbonate data collected near and at the Cheeca Rocks MAPCO2 buoy in the Florida Keys from 2015-01-06 to 2015-12-10* (NCEI Accession 0159154, Version 1.1). NOAA National Centers for Environmental Information. Retrieved from <https://accession.nodc.noaa.gov/0159154>
- Massaro, R. F., De Carlo, E. H., Drupp, P. S., Mackenzie, F. T., Jones, S. M., Shamberger, K. E., et al. (2012). Multiple factors driving variability of CO₂ exchange between the ocean and atmosphere in a tropical coral reef environment. *Aquatic Geochemistry*, 18(4), 357–386. <https://doi.org/10.1007/s10498-012-9170-7>
- McGillis, W. R., Langdon, C., Loose, B., Yates, K. K., & Corredor, J. (2011). Productivity of a coral reef using boundary layer and enclosure methods. *Geophysical Research Letters*, 38, L03611. <https://doi.org/10.1029/2010GL046179>

- McGillis, W. R., Langdon, C., Williams, A. J., & Loose, B. (2009). O₂—MAVS: An instrument for measuring oxygen flux. In *MTS/IEEE Biloxi—Marine technology for our future: Global and local challenges, OCEANS 2009* (pp. 1–9). <https://doi.org/10.23919/OCEANS.2009.5422166>
- McMahon, A., Santos, I. R., Cyronak, T., & Eyre, B. D. (2013). Hysteresis between coral reef calcification and the seawater aragonite saturation state. *Geophysical Research Letters*, *40*, 4675–4679. <https://doi.org/10.1002/grl.50802>
- Meléndez, M., García-Troche, E. M., Morell, J. M., & Salisbury, J. E. (2019). *Dissolved inorganic carbon, total alkalinity, pH, nutrients, and other variables collected from discrete profile observations in the southwest coast of Puerto Rico from 2009-01-16 to 2019-03-07* (NCEI Accession 0188506). NOAA National Centers for Environmental Information. Retrieved from <https://accession.nodc.noaa.gov/0188506>
- Meléndez, M., & Salisbury, J. (2017). Impacts of ocean acidification in the coastal and marine environments of Caribbean small island developing states (SIDS). *Caribbean Mar. Climate Change Rep. Card Sci. Rev.*, *2017*, 31–30. Retrieved from http://72.249.109.29/~uwohxjxf/images/4_Acidification.pdf
- Morelock, J., Ramírez, W. R., Bruckner, A. W., & Carlo, M. (2001). Status of coral reefs, southwest Puerto Rico. *Caribbean Journal of Science Special Publication*, *4*, 57. Retrieved from <https://pdfs.semanticscholar.org/c398/4da3420e66a180c3b873313cb83d7a65457b.pdf>
- Moyer, R. P., Viehman, T. S., Piniak, G. A., & Gledhill, D. (2012). In *Linking seasonal changes in benthic community structure to seawater chemistry*. Paper presented at Proceedings of the 12th International Coral Reef Symposium, Cairns, Australia. Retrieved from http://www.icrs2012.com/proceedings/manuscripts/ICRS2012_8B_1.pdf
- Mucci, A. (1983). The solubility of calcite and aragonite in seawater at various salinities, temperatures, and one atmosphere total pressure. *American Journal of Science*, *283*(7), 780–799. <https://doi.org/10.2475/ajs.283.7.780>
- Muehllehner, N., Langdon, C., Venti, A., & Kadko, D. (2016). Dynamics of carbonate chemistry, production, and calcification of the Florida Reef Tract (2009–2010): Evidence for seasonal dissolution. *Global Biogeochemical Cycles*, *30*, 661–688. <https://doi.org/10.1002/2015GB005327>
- Newton, J. A., Feely, R. A., Jewett, E. B., Williamson, P., & Mathis, J. (2015). *Global ocean acidification observing network: Requirements and governance plan* (2nd ed.). Retrieved from http://www.goa-on.org/documents/general/GOA-ON_2nd_edition_final.pdf
- Olsen, A., Triñanes, J. A., & Wanninkhof, R. (2004). Sea–air flux of CO₂ in the Caribbean Sea estimated using in situ and remote sensing data. *Remote Sensing of Environment*, *89*(3), 309–325. <https://doi.org/10.1016/j.rse.2003.10.011>
- Orr, J. C., Epitalon, J. M., Dickson, A. G., & Gattuso, J. P. (2018). Routine uncertainty propagation for the marine carbon dioxide system. *Marine Chemistry*, *207*, 84–107. <https://doi.org/10.1016/j.marchem.2018.10.006>
- Petraitis, P. S., & Hoffman, C. (2010). Multiple stable states and relationship between thresholds in processes and states. *Marine Ecology Progress Series*, *413*(1), 189–200. <https://doi.org/10.3354/meps08691>
- Pittman, S. J., Hile, S. D., Jeffrey, C. F., Clark, R., Woody, K., Herlach, B. D., et al. (2010). Coral reef ecosystems of Reserva Natural La Parguera (Puerto Rico): Spatial and temporal patterns in fish and benthic communities (2001–2007). *NOAA Technical Memorandum NOS NCCOS*, *107*, 202.
- Precht, W. F., & Miller, S. L. (2007). Ecological shifts along the Florida reef tract: The past as a key to the future. In *Geological approaches to coral reef ecology* (pp. 237–312). New York, NY: Springer. https://doi.org/10.1007/978-0-387-33537-7_9
- Salisbury, J., Vandemark, D., Campbell, J., Hunt, C., Wisser, D., Reul, N., & Chapron, B. (2011). Spatial and temporal coherence between Amazon River discharge, salinity, and light absorption by colored organic carbon in western tropical Atlantic surface waters. *Journal of Geophysical Research*, *116*, C00H02. <https://doi.org/10.1029/2011JC006989>
- Salisbury, J. E., Vandemark, D., Hunt, C. W., Campbell, J. W., McGillis, W. R., & McDowell, W. H. (2008). Seasonal observations of surface waters in two Gulf of Maine estuary–plume systems: Relationships between watershed attributes, optical measurements and surface pCO₂. *Estuarine, Coastal and Shelf Science*, *77*(2), 245–252. <https://doi.org/10.1016/j.ecss.2007.09.033>
- Santos, I. R., Eyre, B. D., & Huettel, M. (2012). The driving forces of porewater and groundwater flow in permeable coastal sediments: A review. *Estuarine, Coastal and Shelf Science*, *98*, 1–15. <https://doi.org/10.1016/j.ecss.2011.10.024>
- Shadwick, E. H., Thomas, H., Azetsu-Scott, K., Greenan, B. J., Head, E., & Horne, E. (2011). Seasonal variability of dissolved inorganic carbon and surface water pCO₂ in the Scotian Shelf region of the Northwestern Atlantic. *Marine Chemistry*, *124*(1–4), 23–37. <https://doi.org/10.1016/j.marchem.2010.11.004>
- Shamberger, K. E. F., Feely, R. A., Sabine, C. L., Atkinson, M. J., DeCarlo, E. H., Mackenzie, F. T., et al. (2011). Calcification and organic production on a Hawaiian coral reef. *Marine Chemistry*, *127*(1–4), 64–75. <https://doi.org/10.1016/j.marchem.2011.08.003>
- Somerfield, P. J., Jaap, W. C., Clarke, K. R., Callahan, M., Hackett, K., Porter, J., et al. (2008). Changes in coral reef communities among the Florida Keys, 1996–2003. *Coral Reefs*, *27*(4), 951–965. <https://doi.org/10.1007/s00338-008-0390-7>
- Sutton, A. J., Feely, R. A., Maenner-Jones, S., Musielwicz, S., Osborne, J., Dietrich, C., et al. (2019). Autonomous seawater pCO₂ and pH time series from 40 surface buoys and the emergence of anthropogenic trends. *Earth System Science Data*, *11*(1), 421–439. <https://doi.org/10.5194/essd-11-421-2019>
- Sutton, A. J., Sabine, C. L., Feely, R. A., Cai, W., Cronin, M. F., McPhaden, M. J., et al. (2016). Using present-day observations to detect when anthropogenic change forces surface ocean carbonate chemistry outside preindustrial bounds. *Biogeosciences*, *13*(17), 5065–5083. <https://doi.org/10.5194/bg-13-5065-2016>
- Sutton, A. J., Sabine, C. L., Maenner-Jones, S., Lawrence-Slavas, N., Meinig, C., Feely, R. A., et al. (2014). A high-frequency atmospheric and seawater pCO₂ data set from 14 open-ocean sites using a moored autonomous system. *Earth System Science Data*, *6*(2), 353–366. <https://doi.org/10.5194/essd-6-353-2014>
- Sutton, A. J., Sabine, C. L., Manzello, D., Musielewicz, S., Maenner Jones, J., Dietrich, C., et al. (2016). High-resolution ocean and atmosphere pCO₂ time-series measurements from mooring Cheeca_80W_25N (NCEI Accession 0157417). NOAA National Centers for Environmental Information. Retrieved from https://doi.org/10.3334/cdiac/otg.cheeca_80w_25n
- Sutton, A. J., Sabine, C. L., Morell, J. M., Musielewicz, S., Maenner, J., Dietrich, S., et al. (2014). *High-resolution ocean and atmosphere pCO₂ time-series measurements from mooring La_Parguera_67W_18N in the Caribbean Sea* (NCEI Accession 0117354). NOAA National Centers for Environmental Information. Retrieved from https://doi.org/10.3334/cdiac/otg.tsm_la_parguera_67w_18n
- Sutton, A. J., Wanninkhof, R., Sabine, C. L., Feely, R. A., Cronin, M. F., & Weller, R. A. (2017). Variability and trends in surface seawater pCO₂ and CO₂ flux in the Pacific Ocean. *Geophysical Research Letters*, *44*, 5627–5636. <https://doi.org/10.1002/2017GL073814>
- Takahashi, T., Olafsson, J., Goddard, J. G., Chipman, D. W., & Sutherland, S. C. (1993). Seasonal variation of CO₂ and nutrients in the high-latitude surface oceans: A comparative study. *Global Biogeochemical Cycles*, *7*(4), 843–878. <https://doi.org/10.1029/93GB02263>
- Takahashi, T., Sutherland, S. C., Sweeney, C., Poisson, A., Metz, N., Tilbrook, B., et al. (2002). Global sea–air CO₂ flux based on climatological surface ocean pCO₂, and seasonal biological and temperature effects. *Deep Sea Research Part II: Topical Studies in Oceanography*, *49*(9–10), 1601–1622. [https://doi.org/10.1016/S0967-0645\(02\)00003-6](https://doi.org/10.1016/S0967-0645(02)00003-6)

- Takeshita, Y. (2017). Understanding feedbacks between ocean acidification and coral reef metabolism. *Journal of Geophysical Research: Oceans*, *122*, 1639–1642. <https://doi.org/10.1002/2017JC012740>
- Takeshita, Y., Cyronak, T., Martz, T. R., Kindeberg, T., & Andersson, A. J. (2018). Coral reef carbonate chemistry variability at different functional scales. *Frontiers in Marine Science*, *5*. <https://doi.org/10.3389/fmars.2018.00175>
- Turk, D., Yates, K. K., Vega-Rodriguez, M., Toro-Farmer, G., Esperance, C. L., Melo, N., et al. (2015). Community metabolism in shallow coral reef and seagrass ecosystems, lower Florida Keys. *Marine Ecology Progress Series*, *538*, 35–52. <https://doi.org/10.3354/meps11385>
- van Heuven, S. M. A. C., Pierrot, D., Rae, J. W. B., Lewis, E., & Wallace, D. W. R. (2011). *MATLAB program developed for CO₂ system calculations, ORNL/CDIAC-105b* (p. 530). Oak Ridge, TN: Carbon Dioxide Information Analysis Center, Oak Ridge National Laboratory, US Department of Energy.
- Venti, A., Andersson, A., & Langdon, C. (2014). Multiple driving factors explain spatial and temporal variability in coral calcification rates on the Bermuda platform. *Coral Reefs*, *33*(4), 979–997. <https://doi.org/10.1007/s00338-014-1191-9>
- Venti, A., Kadko, D., Andersson, A. J., Langdon, C., & Bates, N. R. (2012). A multi-tracer model approach to estimate reef water residence times. *Limnology and Oceanography: Methods*, *10*(12), 1078–1095. <https://doi.org/10.4319/lom.2012.10.1078>
- Wanninkhof, R. (2014). Relationship between wind speed and gas exchange over the ocean revisited. *Limnology and Oceanography: Methods*, *12*(6), 351–362. <https://doi.org/10.4319/lom.2014.12.351>
- Wanninkhof, R., Olsen, A., & Triñanes, J. (2007). Air–sea CO₂ fluxes in the Caribbean Sea from 2002–2004. *Journal of Marine Systems*, *66*(1–4), 272–284. <https://doi.org/10.1016/j.jmarsys.2005.11.014>
- Weiss, R. (1974). Carbon dioxide in water and seawater: The solubility of a non-ideal gas. *Marine Chemistry*, *2*(3), 203–215. [https://doi.org/10.1016/0304-4203\(74\)90015-2](https://doi.org/10.1016/0304-4203(74)90015-2)
- Yeakel, K. L., Andersson, A. J., Bates, N. R., Noyes, T. J., Collins, A., & Garley, R. (2015). Shifts in coral reef biogeochemistry and resulting acidification linked to offshore productivity. *Proceedings of the National Academy of Sciences*, *112*(47), 14,512–14,517. <https://doi.org/10.1073/pnas.1507021112>
- Zeebe, R. E., & Wolf-Gladrow, D. (2001). *CO₂ in seawater: Equilibrium, kinetics, isotopes*, Elsevier Oceanography Book Series (Vol. 65, Issue 1, pp. 1–346). Amsterdam, The Netherlands: Elsevier.